EXPLORING THE SHAPE OF OBJECTS WITH CURVED SURFACES USING TACTILE SENSING

by

Mark A. Charlebois

B.A.Sc. (Systems Design Engineering), University of Waterloo, 1993

A THESIS SUBMITTED IN PARTIAL FULFILLMENT

OF THE REQUIREMENTS FOR THE DEGREE OF

MASTER OF APPLIED SCIENCE

in the School

of

Engineering Science

SIMON FRASER UNIVERSITY

December, 1996

Approval

NAME: Mark Charlebois

DEGREE: Master of Applied Science (Engineering Science)

TITLE OF THESIS: Exploring the Shape of Objects with Curved Surfaces Using Tactile Sensing

EXAMINING COMMITTEE:

Chairman: Dr. Paul Ho

Dr. Kamal Gupta

Senior Supervisor

Dr. Shahram Payandeh

Senior Supervisor

Dr. William Gruver

Supervisor

Dr. John Dill

External Examiner

DATE APPROVED: December 6, 1996

PARTIAL COPYRIGHT LICENSE

Title of Thesis/Project/Extended Essay

"Exploring the Shape of Objects With Curved Surfaces Using Tactile Sensing"

Author:

(signature)

M. Charlebois
(name)

December 6, 1996
(date)

Abstract

An approach to shape description is proposed - called a "Blind Man's" approach - in which tactile information is sensed from the fingertips of a dexterous hand. Using this contact information, two complementary exploratory procedures (EPs) are investigated for curvature estimation and shape description. The first EP (EP1) is based on rolling one finger to estimate curvature at a point on the surface. Montana's equations are used to estimate curvature at a point in simulation and analyze the sensitivity of the approach to noise. The second EP (EP2) uses multiple fingers of a dexterous robot hand to slide along a surface while sensing contact points and surface normals. The surface normal information at the contact points is incorporated into a B-spline surface fit of the data obtained from EP2. Koenderink's shape parameters (S, R) and a confidence estimate of these parameters, are calculated over the B-spline surface.

Acknowledgments

I would like to thank Drs. Shahram Payandeh and Kamal Gupta for their assistance and guidance throughout the course of this research. I would also like to thank Drs. John Dill and Christine Mackenzie for their suggestions and interesting discussion.

Table of Contents

List of Tables

List of Figures

Chapter 1

Introduction

Humans rely heavily on their sense of touch when manipulating objects and gauging depth. Operators have discovered many problems controlling robotic manipulations using only a sense of vision. They have difficulty gauging depth without multiple camera angles which are not always available. Another problem found is that small objects are occluded by the manipulator during manipulation tasks which makes it difficult to find the desired features of the object to grasp, or to orient the object.

Vision systems are also not practical in some hazardous environments. Imagine a room filled with toxic steam which requires a valve to be shut off by a remotely operated robot. A vision system could not provide useful information in such an environment. Using tactile sensing, a robot could orient itself by finding the pipes in the room and then track along the pipe to the valve, find the valve and shut it off. This scenario requires the robot to be able to recognize the pipe and valve objects. The diameter of the pipe may be several times larger than the dexterous hand of the robot. In such a case, would not be possible to recognize the pipe by simply grasping it. The pipe and valve handle are likely to be composed of curved surfaces which are more difficult to recognize than polyhedral objects.

Unlike vision, haptic sensing can extract information about many attributes of an object: shape, mass, volume, rigidity, texture, and temperature to name a few. Human's sense of touch is rich in the amount of information it can acquire simultaneously. However, humans use specialized

Exploratory Procedures (EPs) to extract specific information about an object as described by Klatzky and Lederman [22]. Their investigations also found that shape was the most highly diagnostic property for recognition compared to texture, temperature, and other object properties. They describe a "contour following" EP which humans use to determine the exact and local shape properties of an object.

1.1 Blind Man's Paradigm

In order to examine the extent to which tactile sensing alone can be used to describe an object, a "Blind Man's" approach is adopted in which tactile information from the tips of the fingers is the only sensing modality. This enables the contact point to be sensed and the surface normal to be estimated since the geometry of the fingertip and the configuration parameters of the manipulator are known. In the contect of this thesis, a tactile sensor can be a tactile array, a force/moment sensor, or any other device capable of supplying contact position information.

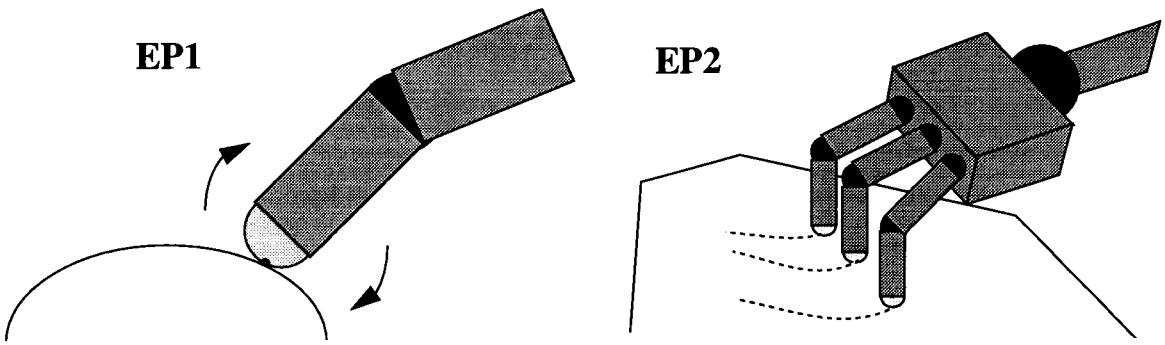

Fig. 1. The Exploratory Procedures: EP1 and EP2

This thesis investigates two EPs (shown in the figure above) for shape perception using fingertip tactile sensors: one based on rolling and the other based on gliding on the surface of the unknown object. Using these two EPs, shape properties at a point on the object and over a patch of the object are explored. My methodology for obtaining more global shape information has been motivated by researchers in computer vision and computer graphics [6], [13], [14], [21], [26], [28], [30] who have investigated aspects of shape description and modelling based on the curvature properties of objects and range images.

Both EPs use a dexterous robot hand with semi-spherical fingertip tactile sensors to probe an object. The curvature at a point on the surface can be estimated from rolling a finger tip on the surface of the object (EP1). The shape properties over a patch on a surface are obtained by sweeping multiple fingers of the dexterous hand across the surface (EP2). The information gathered about the shape of the object could be used to orient the patch, guide further exploratory actions, or be used toward autonomous shape description or object recognition.

The goal of this work was to investigate the use of these two EPs for shape description. The thesis provides the first step in developing a system capable of forming a description of a complex object's shape and recognizing a simple set of objects. Such a system would be required to probe and track the object's surface, determine the shape properties of the tracked region, hypothesize the shape of the patch and test the hypothesis through additional probes.

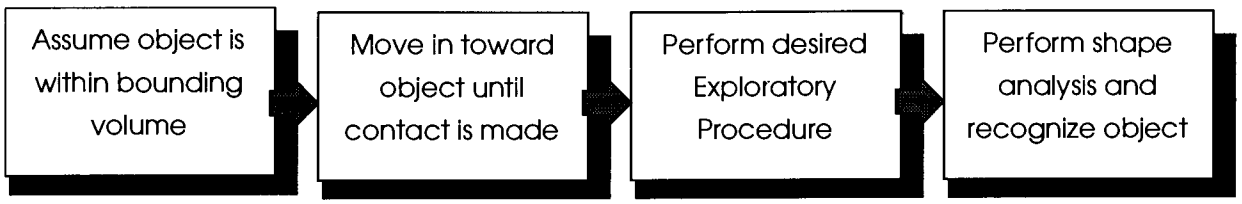

Fig. 2. Flow diagram of the approach

Initially, the object is assumed to be contained within some bounding volume. The hand moves in toward the interior of the box until it makes contact with the object. The desired exploratory procedure is then used to obtain shape information from the object. This thesis addresses only the last two steps in figure 2.

The first exploratory procedure (EP1) involves rolling a single finger on the surface of the object without slipping. Here, several rolling motions are performed in the neighborhood of a contact point. The net rotation of the finger and net displacement of the contact point for each rolling motion are used to determine the curvature in the parametric directions of the probe at the point of interest. EP1 is explained in detail in chapter 3 and several experiments to analyze the sensitivity of the method are presented.

The second exploratory procedure (EP2) uses multiple fingers of a dexterous robot hand to sweep

across the surface of the object. The number of fingers which sweep across the surface is not important although at least two independent traces sweeping in the same direction are required. The contact points are sensed and surface normals are calculated as the fingers sweep across the surface. *A novel approach is used for fitting the B-spline surface patch to the locus of contact points while incorporating the surface normal information.* The degree of the fit is determined by the number of sweeping lines (number of fingers), the length of the sweep across the surface, and the curvature of the class of objects. The data obtained for a patch will be relatively sparse and will also depend on the distance between the fingers. Once the B-spline surface patch has been fit, the curvature and shape properties of the patch can be analyzed. Several experiments are presented which analyze the approximation of the surface, and the shape estimation procedure.

When an object is composed of connected object primitives, multiple regions of the object will have to be probed. If multiple shape primitives exist in a single patch, the patch must be segmented based on the shape primitives being considered. This thesis assumes that the region of the object being probed is composed of only one distinguishable shape primitive. A method to handle multiple shape primitives in a single patch is proposed toward the end of the thesis. The collection of shapes fit to the patches could then be used to perform qualitative model based matching for object recognition. The scope of this thesis is to investigate the feasibility and performance of the method for recognizing the shape primitives from the shape analysis of a patch obtained using EP2.

1.2 Previous Work

This thesis draws on the previous work of researchers in computer vision, computer graphics, tactile sensing, and the kinematics of rolling motion.

1.2.1 Computer Vision

Objects with curved surfaces are described by the curvature at each point on their surface. Some simple objects such as spheres, cylinders, and planes can be recognized from the curvature at a single point. Researchers in computer vision have performed curvature analysis on range images

of objects with curved surfaces [6], [26], [28], [30].

These approaches have all used a segmentation of the image into a region map based on either eight or four shape primitives. A graph based description of the image is composed from its region map. This analysis approach is explained in more detail in chapter 2.

Trucco and Fisher [30] determined the Gaussian and mean curvatures over the surface of a range image. The range image was segmented based on the signs of the Gaussian and mean curvatures The probability of correct classification of points in synthetic patches was then tested. They concluded that qualitative analysis methods were more reliable than quantitative ones for range images. However, they found it was difficult to distinguish between planes and low-curvature surfaces using the zero thresholds for the Gaussian and mean curvatures.

In range image analysis, there are often connected or overlapping objects which have the same shape primitive classification. If two cylinders were connected at right angles they could both be segmented as one object which would be confusing. This problem was addressed by Yokoyo and Levine [30] who computed edge-maps in addition to the curvature based region maps. The discontinuities between object components must eventually be detected when complex objects are sensed using EP2.

A continuous shape parameter has been defined by Koenderink [21] which can also be used to describe an object. He defined a pair of continuous shape parameters (S, R) which describe a surface by its qualitative shape (S) on the interval [-1, 1] and another which represents it's curvedness (C). There are many advantages of the continuous shape description over the traditional HK (Gaussian and mean curvature) sign map approach. Points with similar shape will map to a small interval on the S scale which enables a standard deviation to be calculated. Also, small errors in S will not lead to improper classification of the shape of the point.

1.2.2 Computer Graphics

The basis of B-spline data fitting was presented by DeBoor in [8]. Dierckx [12] has expanded on these formulations to develop several data fitting algorithms including an algorithm for a smoothing spline. This is an iterative algorithm which minimizes changes in the second derivative

based on a smoothing factor which needs to be specified. The fitted curve will become smoother as the value of the smoothing factor increases.

Rogers and Adams [25] provide an excellent overview of B-splines for those unfamiliar with them. For those new to computer graphics, [17] serves as an excellent general reference.

Dill [13] formulated the curvature equations for spline surfaces in a novel way and presented a method for using color to visualize curvature over a surface.

Elber and Cohen [14] describe a way to separate arbitrary surfaces into three disjoint, trimmed surfaces based on a segmentation of convex, concave, and saddle regions. The approach uses a modification of the equation of the determinant of the second fundamental form of the surface which can be represented as a rational function. The positive, zero and negative signs of the determinant are used to partition the surface into the three disjoint trimmed surfaces. The approach is described for Bezier and NURBS representations of a surface.

1.2.3 Tactile Sensing

Researchers have previously investigated recognition of polyhedral objects using tactile sensing. Polyhedral objects can be easily represented by a list of vertex positions, and the vertices which make up a surface. When a polyhedral object is touched there are three distinct features which can be detected: a face, an edge or a vertex. Simple algorithms have been proposed for determining the orientation of a polyhedral object [20], and for recognizing polyhedral objects [24].

Roberts [24] uses the adjacency relations of the sensed features of the object to build an interpretation tree of the feasible matches in the object database. This information is then used to select the next move to test the hypothesized adjacency relations of the known features. Roberts defines three admissible moves and calculates the "cost" of each of these moves in order to determine which type of move to perform next.

Objects with curved surfaces are not as easily described as polyhedral objects. Researchers have previously attempted to recognize very restricted classes of curved objects using tactile sensing. Fearing [15] has investigated recovering shape from extremely sparse tactile data. He attempted to recover a much restricted class of shape models from convex Linear Straight Homogeneous

Generalized Cylinders (LSHGC) from three finger contacts. Using the position, surface normal, and curvature information at the contacts, Fearing attempted to solve the constraint equations of the LSHGC.

Allen and Michelman [1] have investigated tactile sensing EPs to find global shape using superquadrics, to track planar surfaces, and to recognize surfaces of revolution from their contours. The latter EP used a two fingered grasp, moved along the axis of rotation to obtain contour curves on either side of the object. However, the location and axis of the object was determined with human aid.

Fearing and Binford [16] used a cylindrical tactile array to detect the orientation and principal curvatures of a cylindrical object. The contact ellipse is analyzed to determine the orientation of the object and its principal curvatures. The curvature could be estimated within 10% in the direction of the axis of the sensor, but was unreliable in the radial direction. The orientation of the cylinder was determined within 2.5 degrees for a cylinder of radius 25 mm.

1.2.4 Kinematics of Rolling Motion

Montana [23] and Cai and Roth [9] have described kinematic equations for rolling motion between two rigid objects. Cai and Roth [9] introduced basic contact constraints on a point contact between planar curves. Montana's formulation of the kinematic equations is based on the Gauss maps of the surfaces and the Gauss frames at the point of contact. Montana [23] also described a method for estimating the curvature of an object at a point using rolling motions in the neighborhood of the point. Experimental results of the approach for modelling the kinematic motion and determining curvature were not presented in [23].

Hemami, Bay, and Goddard [19] described 2-D gliding and rolling exploration EPs, however their focus was on the sensory requirements for performing these two EPs. They also suggested using the surface normal information to aid in the surface fit of a simple algebraic surface, but no algorithm was provided. Other researchers have described methods for fitting B-spline surfaces [8], [12], [25] to scattered data, but none have provided a formulation to incorporate the surface normals.

1.3 Contribution

There has been very little work done in the field of shape description of objects with general curved surfaces from tactile sensing. This thesis extends the work of other researchers, and provides a framework for describing the shape of an object using tactile sensing.

An analysis of the error sensitivity of Montana's approach is presented. The analysis addresses the limitations of EP1 for a finite resolution sensor and for measurement error of the parameters.

An approach to analyze a curved surface of an object using its surface normal information is presented. A novel method for fitting a B-spline surface to the surface data using the surface normal information is presented along with the experimental results of the method.

This thesis presents an approach for analysis of shape using Koenderink's shape parameter [21] which enables a confidence estimate of the shape parameter to be calculated. The computer vision techniques for describing objects with curved surfaces have not previously been applied to tactile data. The previous approaches also used the signs of the Gaussian and mean curvatures to segment the object into either eight or four classifications (HK sign maps).

1.4 Thesis Layout

There are many ways to analyze the shape properties of a surface which are all indirectly based on the principle curvatures. A detailed explanation of curvature and shape are provided in chapter 2. The benefits of qualitative shape measures are also described.

Chapter 3 provides a detailed description of EP1. The mathematics used to determine the local curvature and the results of sensitivity experiments of the approach are presented.

Chapter 4 provides an overview of EP2 and discusses the motivations for using this approach. A novel B-spline surface fitting algorithm which incorporates the surface normal information is presented. An experimental analysis of the feasibility of this approach for obtaining shape information is performed and its limitations are described.

Chapter 5 describes the experimental results for surface fitting and shape analysis using a physical robot to collect surface data.

Chapter 6 discusses the issues related to the practical implementation of this method, the conclusions of the research and the future directions the research can be taken.

Chapter 2

Background

In order to recognize or describe an object, the features of the object must be determined. These features should be independent of position and orientation. For a polyhedral object these features are the vertices, edges and faces and they can be sensed at a local level. The features of a curved surface of an object that can be locally sensed are less clear. This chapter describes such features for smooth curved surfaces. Local and global shape properties of a surface are explained as well as qualitative shape measures. The following sections of this chapter describe the fundamental equations for evaluating the curvature at a point and how to define shape parameters from the principal curvatures.

2.1 Surface Maps

A surface can be represented as a function of two variables which will be referred to as u and v throughout the thesis. The function f(u, v), called a map, maps the point (u, v) to a point (x, y, z) in R^3. The figure below shows the u-v space which is mapped to the semi-sphere of the tip of a finger by the function $f(u, v)$.

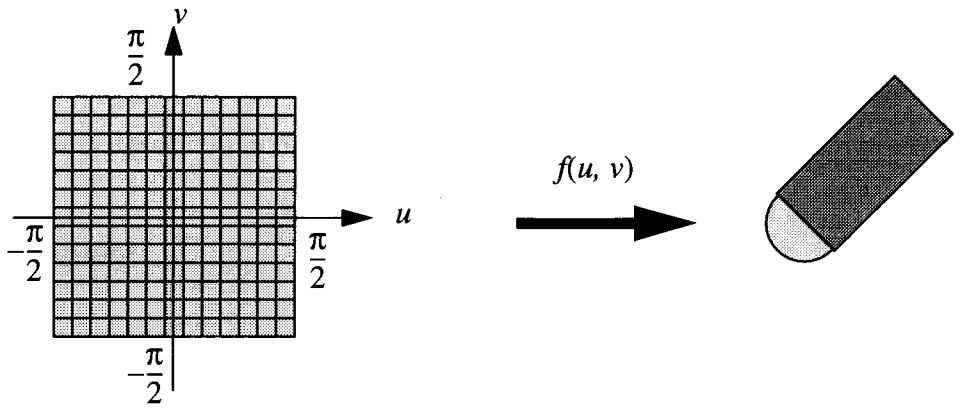

Fig. 3. Surface map $f(u, v)$

The mapping functions for a particular surface are not unique. One map for a semi-sphere with radius R_1 is:

$$f(u,v) = \begin{bmatrix} R_1 \cos u \cos v \\ -R_1 \cos u \sin v \\ R_1 \sin u \end{bmatrix} \qquad \{ (u,v) \mid \left(-\frac{\pi}{2} < u < \frac{\pi}{2}, -\frac{\pi}{2} < v < \frac{\pi}{2} \right) \} \tag{1}$$

2.1.1 Gauss Map

The Gauss map $g(f(u, v))$, maps a point on the surface defined by $f(u, v)$ to the surface normal at that point. This can be quite complex for some shapes which have multiple points on the surface that map to the same surface normal. A torus will have exactly two points on its surface that map to the same surface normal.

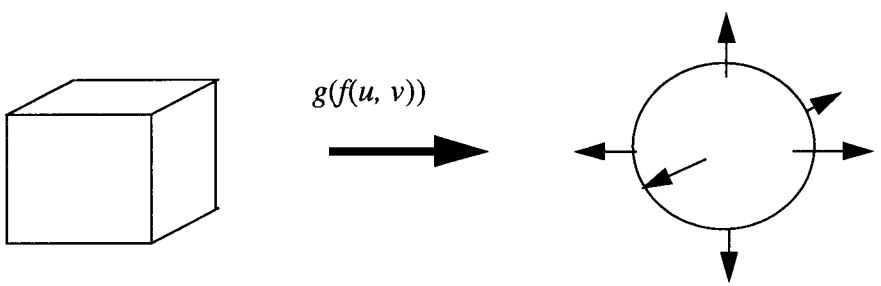

Fig. 4. Gauss map of a cube

As a simple example, the Gauss map for a cube is shown in figure 4. The six faces of the cube map to six points in the Gaussian sphere. The normal at a point on the Gaussian sphere is the vector from the center of the sphere to the point. A method of calculating the Gauss map for an arbitrary surface is described in the following section.

2.1.2 Gauss Frames

The normalized co-ordinate frame at the point of contact (called the Gauss frame) is defined by the following equations:

$$x(u,v) = \frac{f_u(u,v)}{\|f_u(u,v)\|} \qquad y(u,v) = \frac{f_v(u,v)}{\|f_v(u,v)\|} \qquad z(u,v) = g(f(u,v)) \tag{2}$$

The Gauss map for an arbitrary surface map can be calculated as the cross product of $x(u, v)$ and $y(u, v)$.

$$z(u,v) = g(f(u,v)) = x(u,v) \times y(u,v) \tag{3}$$

When two objects are in contact, a Gauss frame is defined at the point of contact for each object. The normals at the point of contact are colinear and have opposite signs. The x and y-axes of the two Gauss frames lie in the same plane, but will likely not be aligned and they will be offset by some rotation angle (ψ) around the z-axis. The following figure shows the Gauss frames for two objects in contact. The individual Gauss frames are shown and then they are superimposed showing the angle between them.

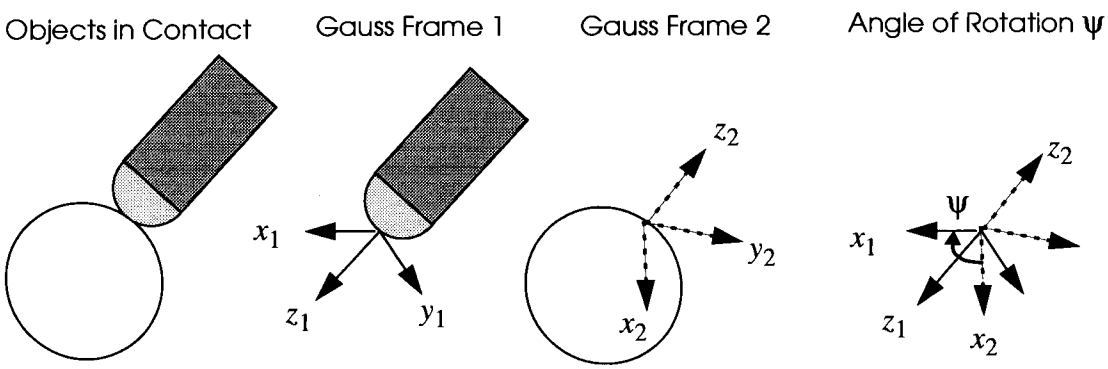

Fig. 5. Rotation angle between Gauss frames for two object in contact

2.1.3 The Metric

The metric of the surface is used to measure the changes in the position on the surface for a differential change in the parameters u and v. The general equation for the metric of the surface is:

$$M_1 = \begin{bmatrix} \|f_u(u, v)\| & 0 \\ 0 & \|f_v(u, v)\| \end{bmatrix} \tag{4}$$

For a further discussion of the metric of a surface see p. 225 in [21].

2.2 Curvature

Local shape properties are determined completely by the *principal curvatures* at a point on the surface. Curvature is a measure of the rate of change of the surface normal in a particular direction at a point on the surface. The shape of a patch does not depend on its orientation or location in space. There are many ways to analyze and represent the curvature at a point on the surface. The different types of curvature are defined in the following sub-sections.

2.2.1 The Normal Curvature

On a general surface $Q(u, v)$, the direction of the surface normal of an object changes as you move across the surface. A mathematical description of the normal curvature is provided in this section.

Consider a surface $Q(u, v)$. The unit normal is defined as:

$$\bar{n} = \frac{\frac{\partial Q}{\partial u} \times \frac{\partial Q}{\partial v}}{\left| \frac{\partial Q}{\partial u} \times \frac{\partial Q}{\partial v} \right|} \tag{5}$$

The normal curvature at a point (u, v) varies as a function of the direction of the differential vector (du, dv) shown in the diagram below.

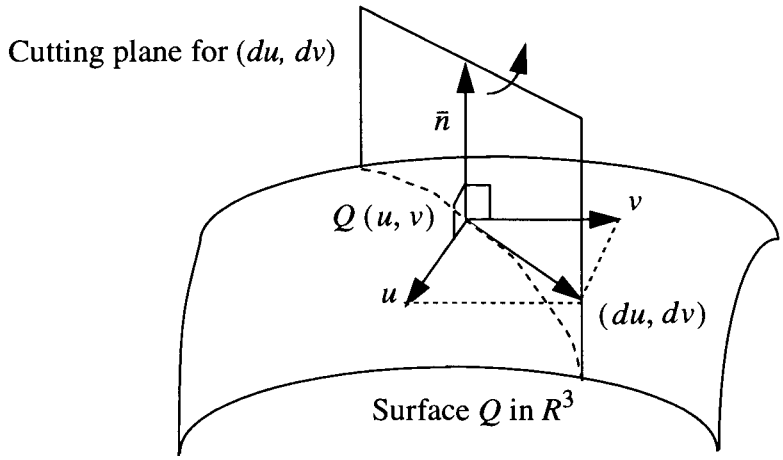

Fig. 6. Graphical depiction of normal curvature

In order to simplify the equations for curvature, the variables E, F, G, and e, f, g have been defined as the following dot products:

$$\begin{aligned} E &= \frac{\partial Q}{\partial u} \bullet \frac{\partial Q}{\partial u} \qquad F = \frac{\partial Q}{\partial u} \bullet \frac{\partial Q}{\partial v} \qquad G = \frac{\partial Q}{\partial v} \bullet \frac{\partial Q}{\partial v} \\ e &= \frac{\partial^2 Q}{\partial u^2} \bullet \bar{n} \qquad f = \frac{\partial^2 Q}{\partial u \partial v} \bullet \bar{n} \qquad g = \frac{\partial^2 Q}{\partial v^2} \bullet \bar{n} \end{aligned} \tag{6}$$

The first fundamental form measures the differential movement on the surface for a differential movement in the parameter plane [6]. The first fundamental form is defined as:

$$I(u, v, du, dv) = \begin{bmatrix} du & dv \end{bmatrix} \begin{bmatrix} E & F \\ F & G \end{bmatrix} \begin{bmatrix} du \\ dv \end{bmatrix} = \begin{bmatrix} du & dv \end{bmatrix} \begin{bmatrix} M \end{bmatrix} \begin{bmatrix} du \\ dv \end{bmatrix} \tag{7}$$

where the M matrix is the metric of the surface.

The second fundamental form is defined as:

$$II(u, v, du, dv) = \begin{bmatrix} du & dv \end{bmatrix} \begin{bmatrix} e & f \\ f & g \end{bmatrix} \begin{bmatrix} du \\ dv \end{bmatrix} \tag{8}$$

The normal curvature for a given point on the surface (u, v) is defined as:

$$Kn = \frac{edu^2 + 2fdudv + gdv^2}{Edu + 2Fdudv + Gdv^2} = \frac{II}{I} \tag{9}$$

The normal curvature in a particular tangent direction is the reciprocal of the radius of curvature in that direction. The above definition of the normal curvature allows us to find the curvature at a point in any arbitrary tangential direction. This feature will be used to determine the principal curvatures at the point of interest.

2.2.2 Determining Principal Curvatures

The curvature at a point is characterized by the principle curvature directions and the magnitudes of curvature in each direction. Imagine that the cutting plane in the previous figure was rotated through a complete circle and the normal curvature was calculated in every direction. There would be a minimum and maximum value for the normal curvature associated with two separate directions. In special cases like a sphere, the normal curvature is the same in all directions so the principal curvatures are identical and have no unique directions. A point with this property is called an *umbilic point.*

The directions of minimum and maximum normal curvature are the *principal directions* of curvature. The *Gaussian curvature* (Kg) is the product of the minimum and maximum curvatures and the *mean curvature* (Ka) is simply their average. The Gaussian and mean curvatures can be easily calculated using the following equations. A more complete description can be found in [4], [13], [14] and [26].

The Gaussian and mean curvature are then respectively:

$$Kg = \frac{(eg - f^2)}{(EG - F^2)} \qquad Ka = \frac{(Eg - 2Ff + Ge)}{2(EG - F^2)} \tag{10}$$

If the direction of the principal curvatures is not required to be known, the minimum and maximum curvatures can be determined from the Gaussian and mean curvatures by:

$$Kmax = Ka + \sqrt{Ka^2 - Kg}$$
$$Kmin = Ka - \sqrt{Ka^2 - Kg} \tag{11}$$

The method to determine the directions of principal curvature associated with the principal curvatures is described in the following section.

2.2.3 Determining the Directions of Principal Curvature

An example of when the directions of minimum and maximum curvature may be required, is calculating the curvature flow lines over a patch. The equations for calculating the minimum and maximum curvature directions are:

$$\begin{bmatrix} \dot{u} \\ \dot{v} \end{bmatrix} = \begin{bmatrix} \frac{1}{2}(Eg - Ge) + \left(EG - F^2\right)\sqrt{Ka^2 - Kg} \\ Fe - Ef \end{bmatrix}, minimum$$
$$\begin{bmatrix} \dot{u} \\ \dot{v} \end{bmatrix} = \begin{bmatrix} Gf - Fg \\ \frac{1}{2}(Eg - Ge) + \left(EG - F^2\right)\sqrt{Ka^2 - Kg} \end{bmatrix}, maximum \tag{12}$$

The directions of curvature are also useful to determine the orientation of certain object primitives. If the directions of principal curvature are known for a cylinder, then the orientation of the axis of the cylinder can be determined.

2.2.4 Curvature Form

The curvature form (K) of the surface is defined as:

$$K = \begin{bmatrix} x(u,v)^T \\ y(u,v)^T \end{bmatrix} \begin{bmatrix} \frac{z_u(u,v)}{\|f_u(u,v)\|}, & \frac{z_v(u,v)}{\|f_v(u,v)\|} \end{bmatrix} = \begin{bmatrix} h_1 & h_2 \\ h_2 & h_3 \end{bmatrix} \tag{13}$$

The curvature form of a surface is a 2 x 2 symmetric matrix that measures the rate of change of the surface normal with respect to u and v projected on the x and y-axes of the Gauss frame. The rates of change of the surface normal in the u direction and v direction are $z_u(u, v)$ and $z_v(u, v)$

respectively.

The element h_1 measures $z_u(u, v)$ projected on the x-axis, divided by the metric for the u parameter. Similarly, h_3 measures $z_v(u, v)$ projected on the y axis, divided by the metric for the v parameter. The off-diagonal elements (h_2) measure the twist of the normal.

2.3 Space Curves, Arc Length, and Torsion

Consider a parametric space curve $h(t)$ in R^3 as shown in figure 7. Let the unit tangent at a point t on the curve be $T(t)$. Let the unit normal be $N(t)$. Let the unit binormal, the cross product of the tangent and the normal, be $B(t)$. Together, the tangent, normal and binormal form a orthogonal frame a the point on the curve. As t increases, the point moves along the curve and the frame at the point will twist as the instantaneous center of curvature changes.

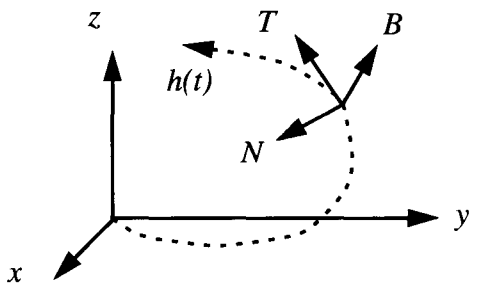

$$h(t) \Rightarrow (x, y, z) \in R^3$$

$$B(t) = T(t) \times N(t)$$

Fig. 7. The tangent (T), normal (N) and binormal (B) of the curve

2.3.1 Arc Length

The distance between two points on a space curve is not measured as the Euclidean distance. Instead, the arc length is used to measure the distance along the curve as if it were straightened out and measured. The arc length (s) of a parametric space curve from t_0 to t_1 is defined as:

$$s(t_1) = \int_{t_0}^{t_1} \sqrt{\left(\frac{dx}{dt}\right)^2 + \left(\frac{dy}{dt}\right)^2 + \left(\frac{dz}{dt}\right)^2}\, dt \qquad (14)$$

2.3.2 Torsion

The torsion of a curve (τ) measures how much the curve twists. The torsion is always in the direction of the normal and measures the rate of change of the binormal for an differential change in arc length of the curve.

$$\frac{dB}{ds} = -\tau N \tag{15}$$

2.3.3 Torsion Form

The torsion form of a surface is a vector which is analogous to the torsion of a curve defined above. The torsion form measures the twist of the x-axes of the Gauss frame in the u-direction and in the v-direction at a point on the surface.

$$T = y(u,v)^T \left[\frac{x_u(u,v)}{\|f_u(u,v)\|}, \quad \frac{x_v(u,v)}{\|f_v(u,v)\|} \right] \tag{16}$$

2.4 Qualitative Shape Properties

"Intuitively, *shape* is how the normal-or equivalently the tangent plane-turns as you move in arbitrary directions over the surface." - J. J. Koenderink [21]

The shape properties at a point can be represented by the principal curvatures, or the Gaussian and mean curvatures at that point. However, these quantitative values do not capture the essence of the shape of the surface. Regardless of the size of a sphere, all spheres have the same shape. "Shape" is a quality, "size" is the quantity.

Researchers in computer graphics and image processing have previously tried to describe the shape of objects using qualitative shape measures. The positive and negative signs of the Gaussian and mean curvatures (*Kg* and *Ka*) yield a set of four surface primitives. A surface can be segmented into regions based on these primitives which will produce a region map of the surface. The table below shows the signs of the Gaussian and mean curvatures and the associated shape

primitives.

Table 1: Shape Primitives for Positive and Negative Gaussian and Mean Curvatures

Shape	*Kg*	*Ka*
Saddle Valley	Negative	Negative
Saddle Ridge	Negative	Positive
Concave	Positive	Negative
Convex	Positive	Positive

Alternatively, a zero threshold for the Gaussian and mean curvatures can be used which yields a set of eight shape primitives [11]. The following table shows the signs of the Gaussian and mean curvatures and the associated shape primitives.

Table 2: Shape Primitives for Positive, Negative and Zero Gaussian and Mean Curvatures

Shape	*Kg*	*Ka*
Saddle Valley	Negative	Negative
Minimal Saddle	Negative	Zero
Saddle Ridge	Negative	Positive
Valley	Zero	Negative
Flat	Zero	Zero
Ridge	Zero	Positive
Pit	Positive	Negative
Peak	Positive	Positive

Notice in the above table that there is no entry for a positive *Kg* and a *Ka* of zero. The Gaussian curvature cannot be positive when the mean curvature is zero by definition.

2.4.1 A Continuous Shape Descriptor

The shape primitives defined in the previous section are qualitative measures. However, these shape primitives have the deficiency of being discrete. Koenderink [21] proposes an alternative continuous representation of shape using two parameters: R and S. The definitions of these

parameters are as follows.

$$R = \sqrt{\frac{(Kmin^2 + Kmax^2)}{2}} \qquad S = -\frac{2}{\pi}\operatorname{atan}\left(\frac{Kmax + Kmin}{Kmax - Kmin}\right) \tag{17}$$

The S parameter represents the shape and the R parameter represents the curvedness of the patch. Spheres would have an S value of exactly one. The size of the sphere would determine its R value. A plane would have an R value of zero and it's S value would be undefined.

The following figure shows how the S parameter maps the shapes into the interval [1,1].

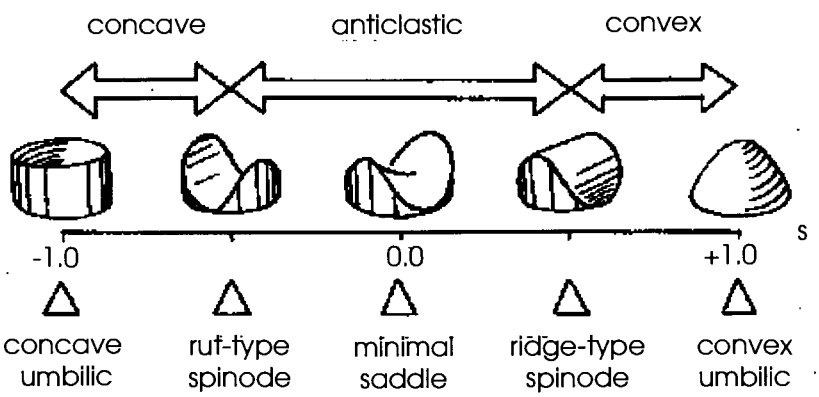

Fig. 8. Koenderink's Shape Parameter (from Solid Shape by J. Koenderink, MIT press, 1990)

A convex umbilic is another term for a spherical point. Every point on the surface of a sphere is a convex umbilic because the minimum and maximum curvatures are the same in every direction. A concave umbilic is the hole a sphere would leave if it were dropped in soft ground.

Koenderink's representation for S equal to zero can be somewhat confusing. Minimal points on a surface have a mean curvature of zero which means K_{min} is equal to $-K_{max}$. The S parameter is equal to zero for minimal points where the principal curvatures are non-zero. The S parameter is not defined at planar points. The family of saddles defined by $z = Ax^2 - Ay^2$ have minimal points (S equal to 0) along the lines $y=x$ and $y=-x$. However, all other points on the saddle surfaces correspond to an S value other than zero.

Some simple surfaces have the same S values everywhere. The following table shows some

expected values of S for various primitive shapes.

Table 3: Expected Values of S for Various Shapes

Shape	Expected Value of S
Sphere	1.0
Convex Cylinder Section	0.5
Concave Cylinder Section	-0.5
Spherical Pit	-1.0

Koenderink proposed an alternative curvedness parameter to R which maps the domain $[0, \infty]$ to $[-\infty, \infty]$. The new equation of the curvedness parameter is

$$C = \frac{2}{\pi}\log(R) . \tag{18}$$

The following figure shows the combination of the S and C parameters.

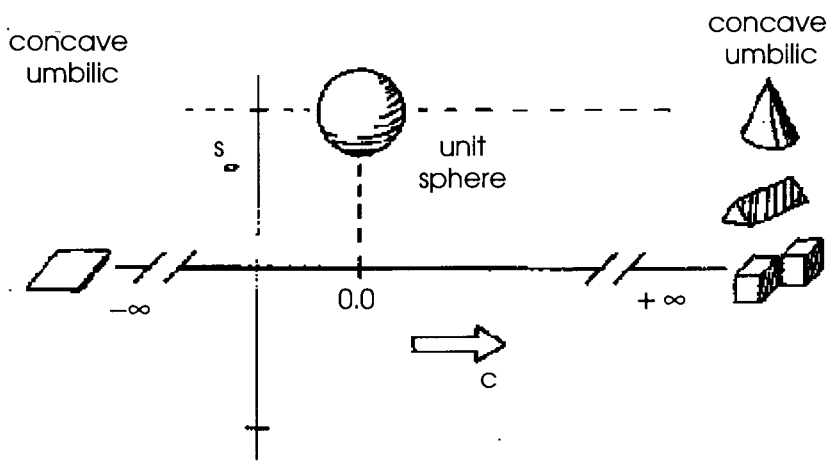

Fig. 9. Koenderink's Shape and Curvedness Parameters (from Solid Shape by J. Koenderink, MIT press, 1990)

For example, a sphere has a shape parameter $S = 1.0$. The C parameter will change based on the radius of the sphere. A point on a sphere with a very large radius will be nearly planar, and the value of C will tend toward $-\infty$ as the radius of the sphere increases.

Chapter 3

EP1

This chapter provides an overview of the first exploratory procedure (EP1) which is used to estimate local curvature at a point on the surface of an object. EP1 uses one finger of a dexterous robot hand to perform rolling motions on the surface of an object in the neighborhood of a point on the surface. The curvature of the object at that point is determined from the rolling motions. This chapter provides a detailed description of how the curvature at a point on the surface is determined using EP1. The approach for curvature calculation is based on Montana's [23] kinematic equations of rolling motion between two rigid objects.

Simulation studies have been performed which analyze the sensitivity to error of this approach for determining curvature. A summary of the findings is presented along with a discussion of the details which must be considered in order to implement this method.

3.1 Overview

The surface curvature at a point can be estimated from small rolling motions (which will be referred to as probes) in the neighborhood of the contact point. Montana [23] derived the kinematics for two rigid bodies in rolling contact and described a method to determine the surface curvature at a point. This approach has been verified in simulation and analyzed for its sensitivity to measurement error and sensor resolution.

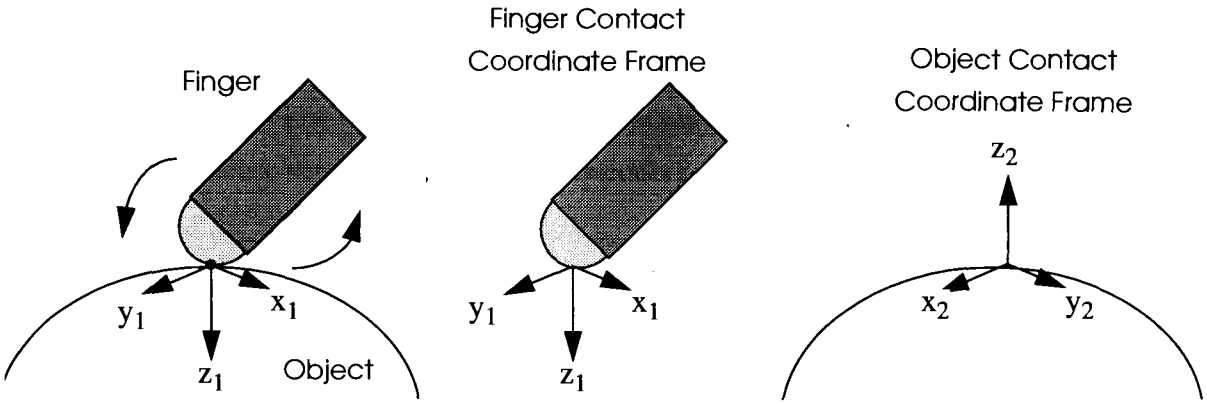

Fig. 10. The contact frames for the finger and object

Using this approach, the finger is required to rotate a desired amount around the x or y-axis in the instantaneous contact frame of the fingertip. The surface of the fingertip is parameterized by u and v based on its Gauss map. The contact frame will be determined by the point of contact, the surface normal, and the initial contact configuration (see figure 10). The surface normal at the point of contact can be determined from the Gauss map when the geometry of the fingertip is known. A semi-spherical fingertip was used in the following simulations for simplicity.

The algorithm for analyzing a surface using EP1 is as follows:

1. Roll the fingertip along the surface of the object without slipping by rotating positively about the instantaneous x-axis for a desired rotation ($\Delta\theta$) of the finger
2. Record the net displacement of the contact point (Δp).
3. Roll the fingertip back to the initial position by rotating in the opposite direction about the instantaneous x-axis for a desired net rotation of the finger
4. Record the net displacement of the contact point (Δp).
5. Repeat steps 1 to 4 by rotating negatively about the x-axis, positively about the y-axis, and negatively about the y-axis. This will have traced a "+" pattern centered at the initial contact point.
6. Calculate the curvature form based on the Montana's kinematic equation of relative rolling motion using the recorded values of $\Delta\theta$ and Δp.

7. Estimate the radii of curvature in x and y directions of the probe from the curvature form.

The method for determining the curvature of the object at a point using EP1 will be described in detail in the sections below. The accuracy of the calculation of the curvature will depend on the resolution of the tactile sensor, the robot joint encoders, the arc length of the rolling motion, and the calibration of the robot.

The following definitions will be used throughout the remainder of this chapter.

3.1.1 Definitions

Let $\Delta\theta_x$ and $\Delta\theta_y$ be the approximations of the sums of the instantaneous rotations about the x-axis and y-axis of the instantaneous contact frames for a particular probe.

Let $\Delta p_1 = (\Delta u_1, \Delta v_1)$ be the change in the coordinates of the contact point on the surface of the probe.

Let Δs be the length of the curve traced on the surface of the probe for a particular rolling motion. The evolution of the contact point on the probe as it rolls on the surface of the object is used to determine the curvature in the direction of motion. Probes in two independent directions are sufficient to determine the curvature although, if more probes are performed a least squares fit can be calculated for greater confidence.

Let the relative curvature ratio (RCR) be defined as the normal curvature of the probe at the point of contact in a particular tangent direction divided by the normal curvature of the object in the same direction. This is equivalent to the radius of curvature of the probe divided by the radius of curvature of the object. As the relative radius of the object increases, the RCR increases.

$$\frac{Kn_{probe}}{Kn_{object}} = \frac{R_{object}}{R_{probe}} \tag{19}$$

3.2 Determining Local Curvature from Rolling

Montana's kinematic equations of rolling motion between two rigid objects are used to estimate

the curvature form at a point on the surface.

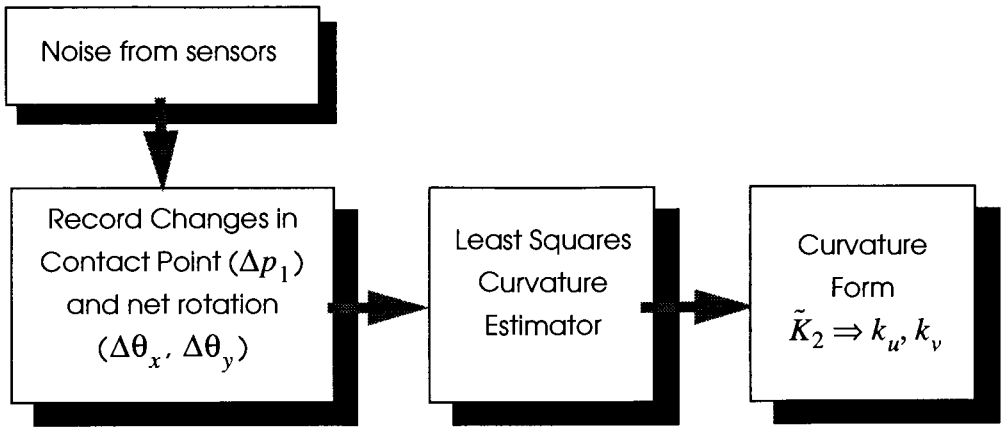

Fig. 11. Input and output of the curvature estimator

The curvature form at a point on the surface is estimated from eight probes: two in each of the u, -u, v, and -v directions. The direction of the probes is shown in the figure below. The eight samples of $\Delta\theta_x$, $\Delta\theta_y$, and Δp_1 are used to determine the minimum error solution of the curvature form. Figure 11 shows the inputs and outputs of the curvature estimation procedure. The returned values k_u and k_v are the normal curvatures in the u and v directions.

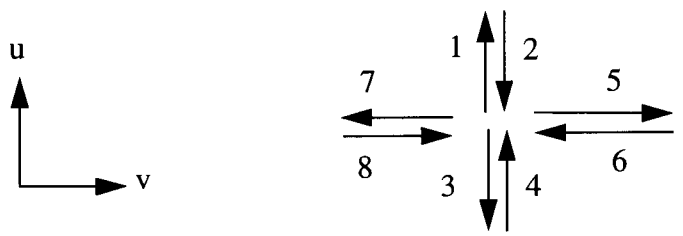

Fig. 12. The eight probing motions used to estimate the curvature at a point

The $\Delta\theta_x$ and $\Delta\theta_y$ parameters are calculated by measuring the net rotation with respect to the initial contact frame. Figure 13 shows a 90 degree rotation of the finger ($\Delta\theta$) on planar and spherical surfaces. In the planar case, the surface normal points in the same direction in both the initial and final positions. In the spherical case, the direction of the surface normal has rotated 45 degrees since the sphere has the same radius as the fingertip. In the case of convex surfaces, the angular rotation of the surface normal will be less than for a planar surface for the same $\Delta\theta$. The curvature

estimation is based on the difference in the change in the contact point for a known angular rotation of the finger.

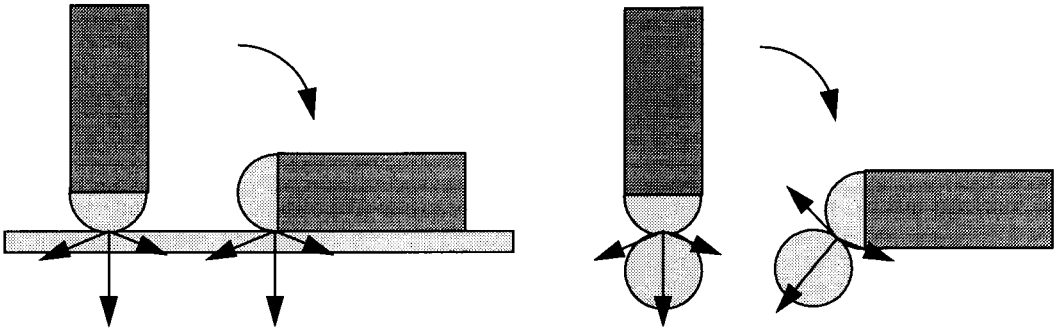

Fig. 13. Angular rotations of $\frac{\pi}{2}$ for a planar surface and a sphere of radius 1

The following section describes the formulation for the parameterization of the fingertip and how to use Montana's equations for calculating the curvature at a point.

3.2.1 Parameterization of the Probe Geometry

The surface of the fingertip can be parameterized by two variables: u and v. The parameterization or map, of the semi-sphere was selected to be the same as that used by Montana for a sphere however, any parameterization can be used.

The map for the semi-sphere with radius R_1 is:

$$f(u, v) = \begin{bmatrix} R_1 \cos u \cos v \\ -R_1 \cos u \sin v \\ R_1 \sin u \end{bmatrix} \qquad \{ (u, v) \mid \left(-\frac{\pi}{2} < u < \frac{\pi}{2}, -\frac{\pi}{2} < v < \frac{\pi}{2} \right) \} \tag{20}$$

This map is chosen to make the Gauss map equation simple. As described in chapter 2, the Gauss map $g(f(u, v))$, maps the point on the surface defined by $f(u, v)$ to the surface normal at that point.

The Gauss map for the above surface map is:

$$g(f(u, v)) = (\cos u \cos v, -\cos u \sin v, \sin u) \tag{21}$$

which is simply $f(u,v)/R_1$ in the case of a spherical region.

The Gauss frame for the semi-sphere is defined by:

$$x(u,v) = \begin{bmatrix} -\sin u \cos v \\ \sin u \cos v \\ \cos u \end{bmatrix} \qquad y(u,v) = \begin{bmatrix} -\sin v \\ -\cos v \\ 0 \end{bmatrix} \qquad z(u,v) = \begin{bmatrix} \cos u \cos v \\ -\cos u \sin v \\ \sin u \end{bmatrix} \tag{22}$$

The metric for the surface is used to measure the changes in the position on the surface for a differential change in the parameters u and v.

The metric, curvature form, and torsion form for the semi-sphere are:

$$M_1 = \begin{bmatrix} R_1 & 0 \\ 0 & R_1 \cos u \end{bmatrix} \qquad K_1 = \begin{bmatrix} \frac{1}{R_1} & 0 \\ 0 & \frac{1}{R_1} \end{bmatrix} \qquad T = \begin{bmatrix} 0 & \frac{-\tan u}{R_1} \end{bmatrix} \tag{23}$$

The resulting curvature form is a diagonal matrix with $1/R_1$ on the diagonal.

The metric, and curvature form of the probe are required to solve for the curvature form of the object. The torsion form of the probe is used to simulate the rolling motion of two rigid objects. The following section describes Montana's kinematic equations for the rolling motion between two rigid objects which requires the quantities defined above.

3.2.2 Montana's Equations of Motion

The following are the equations for the kinematics of a rigid probe and rigid object in rolling contact and is based on the Gauss maps of both objects. This equation was used to simulate the motion of the rolling fingertip probe on the surface of the unknown object. The contact point on the probe evolves according to the following differential equation of motion:

$$\frac{dp_1}{dt} = M_1^{-1}\left(K_1 + \tilde{K}_2\right)^{-1}\left(\begin{bmatrix} -\omega_y \\ \omega_x \end{bmatrix} - \tilde{K}_2 \begin{bmatrix} \upsilon_x \\ \upsilon_y \end{bmatrix}\right) \tag{24}$$

where:

K_1 is the known curvature form of the probe

$\tilde{K}_2$ is the curvature form of the object in the probe's contact frame

M_1 is the metric of the probe

$\omega = [\omega_x , \omega_y]$ is the vector containing the angular velocities of the probe's contact frame with respect to the object's contact frame around the x and y-axis

υ_x and υ_y are the linear velocities of the probe's contact frame with respect to the object's contact frame in the x and y direction

p_1 is the contact point (u_1, v_1) on the probe

The differential equation for the motion of the contact point on the object is:

$$\frac{dp_2}{dt} = M_2^{-1} R_\psi \left(K_1 + \tilde{K}_2 \right)^{-1} \left(\begin{bmatrix} -\omega_y \\ \omega_x \end{bmatrix} - K_1 \begin{bmatrix} \upsilon_x \\ \upsilon_y \end{bmatrix} \right) \tag{25}$$

where in addition to the above:

M_2 is the metric of the object

R_ψ is the orientation of the x and y-axes of the probes contact frame relative to the x and y-axes of the objects contact frame

p_2 is the contact point $[u_2, v_2]$ on the object.

The orientation matrix is defined as:

$$R_\psi = \begin{bmatrix} \cos\psi & -\sin\psi \\ -\sin\psi & -\cos\psi \end{bmatrix} \tag{26}$$

where

$$\dot{\psi} = w_z + T_1 M_1 \dot{p}_1 + T_2 M_2 \dot{p}_2 \tag{27}$$

The sign of ψ is chosen such that a rotation of the probe's contact frame through an angle of $-\psi$ around its z-axis aligns the x-axis of its frame with the x-axis of the object's contact frame.

The arc length (Δs) is defined as:

$$\Delta s = \int_{t_0}^{t_1} \left(K_1 + \tilde{K}_2 \right)^{-1} \left(\begin{bmatrix} -\omega_y \\ \omega_x \end{bmatrix} - K_1 \begin{bmatrix} \upsilon_x \\ \upsilon_y \end{bmatrix} \right) dt \tag{28}$$

The arc length will be the distance of the path travelled by each of the rolling probes.

A visual simulation of the fingertip of a dexterous hand rolling on a sphere was created as a secondary check of the implementation of these equations. An implementation of Montana's method could not be found in the literature, so a verification was necessary. The simulation performed a probes which formed a "+" pattern, centered at a point on the surface. These probes were used to determine the curvature form of the sphere. The user could set the size of the sphere using the mouse and the radius of the sphere could be calculated. A picture of this simulation is shown in figure 14.

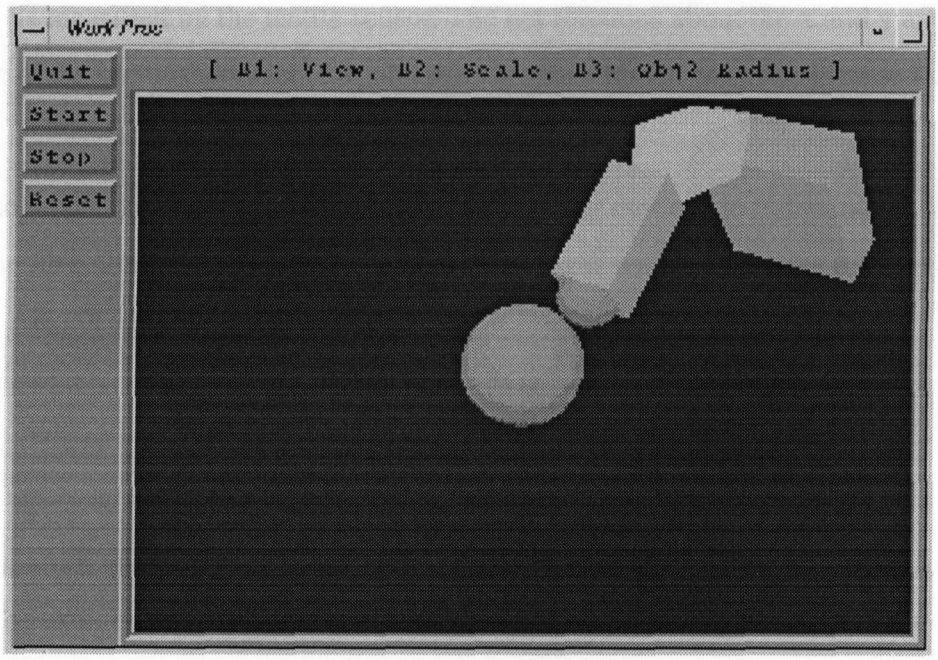

Fig. 14. Graphical simulation of the finger of the dexterous hand rolling on the object

The simulation verified that the equations gave the expected results and helped give some visual understanding to the equations. Once a clear understanding of the parameters was gained, the

sensitivity of the approach for curvature estimation was tested. The following section describes how the curvature is estimated.

3.2.3 Curvature Estimation from Rolling Probes

Montana described an approach to determine the curvature at a point on an object using the kinematic equations for rolling motion between two rigid objects. The approach requires that the fingertip rolls on the object without slipping. For rolling contact (i.e. no slipping), $\upsilon_x = \upsilon_y = \upsilon_z = 0$ in equation (24) above. The angular rotation about the contact normal (ω_z) must also be zero. Equation (24) can be approximated by:

$$M_1 \Delta p_1 + e_i = \left(K_1 + \tilde{K}_2 \right)^{-1} \begin{bmatrix} -\Delta\theta_{y_i} \\ \Delta\theta_{x_i} \end{bmatrix} \tag{29}$$

It is assumed that $\tilde{K}_2$ will not change significantly if Δp is small. The change in the point of contact Δp_1 is measured by the tactile sensor. The net rotations about the x and y axes of the Gauss frame at the point of contact ($\Delta\theta_x$ and $\Delta\theta_y$) are determined from the inverse kinematics of the robot.

In order to solve for the curvature form, at least two rolling motions in independent directions are required. The *i*th rolling motion requires rotating the finger without slippage through a small angle $\left[\Delta\theta_{x_i} \; \Delta\theta_{y_i} \; 0\right]^T$.

$$\Delta\theta = \int_{t0}^{t1} \omega(t)\, dt \approx \sum_{i=1}^{n} \omega_i \Delta t = n\omega_{avg} \Delta t \tag{30}$$

The approximation in equation (30) assumes the axis remains parallel to the initial configuration throughout the extent of the rolling motion. If the direction of rolling follows the *u* or *v* lines of the surface or the surface has constant curvature, then the approximation is identical to the actual rotation. Otherwise, the approximation will not be exact because the axis of rotation will no longer be parallel to its initial configuration as the point of contact moves along the surface. This will be discussed in more detail later in section 3.3.1.

Determining the curvature of the unknown object requires solving equation (29) for the unknown curvature form $\tilde{K}_2$. Since the inverse of the relative curvature form is symmetric:

$$\left(K_1 + \tilde{K}_2\right)^{-1} = \begin{bmatrix} k_1 & k_2 \\ k_2 & k_3 \end{bmatrix} \tag{31}$$

The least squares solution for these unknown values can be solved using the following equation:

$$\begin{bmatrix} k_1 & k_2 & k_3 \end{bmatrix}^T = \left(A^T A\right)^{-1} A^T B \tag{32}$$

where

$$A = \begin{bmatrix} -\Delta\theta_{y_1} & \Delta\theta_{x_1} & 0 \\ 0 & -\Delta\theta_{y_1} & \Delta\theta_{x_1} \\ \cdots & \cdots & \cdots \\ -\Delta\theta_{y_n} & \Delta\theta_{x_n} & 0 \\ 0 & -\Delta\theta_{y_n} & \Delta\theta_{x_n} \end{bmatrix} \qquad B = \begin{bmatrix} M_1 \Delta p_{1_1} \\ \cdots \\ M_1 \Delta p_{1_n} \end{bmatrix}. \tag{33}$$

Once the values of k_1, k_2, and k_3 are solved, equation (31) can be used to solve for $\tilde{K}_2$. The diagonal elements of $\tilde{K}_2$ are the normal curvatures in the u and v directions.

The solution, is only

3.3 Simulation Studies

Simulation experiments were performed to analyze the sensitivity of EP1 for estimating curvature from rolling when error in the measurement of $\Delta\theta$ is present. A semi-spherical fingertip with a radius of 1 unit (R_1) was rolled on spheres of various radii in simulation. The curvature of the spheres was estimated for various finger rotations $\Delta\theta$. The curvature estimation is affected by the arc length (Δs) of the probe which is related to the net rotation for a particular RCR. Δs varies for a given rotation of the finger as the RCR changes. There are four sources of error in the estimation procedure: (i) measuring the angular rotation, (ii) the resolution of the contact sensor, (iii) the

relative curvature ratio, and (iv) the length of Δs.

The first and second sets of simulations show the relation between the estimation error, the RCR and the sensitivity to noise for objects with constant and varying curvature.

The third set of simulations show the effect of the resolution of the contact sensor on the error in the curvature estimation.

3.3.1 Angular Rotation Error

There are many sources of error which could affect the accuracy of the measurement of the angular rotation of the probing motion. The measurement will depend on the accuracy of the tactile sensor, the accuracy of the robot encoders and the accuracy of the kinematic model of the robot. The sensitivity of EP1 to angular rotation measurement error was analyzed by adding a noise values in the direction of each rolling motion.

The rotation matrix which transforms vectors in the finger co-ordinate frame to the world frame is determined from the inverse kinematics of the robot. A detailed explanation of this can be found in [27]. Let Rot_1 be the rotation matrix which transforms the surface normal $z(u_0, v_0)$, to the world frame for the initial configuration of the robot. Let Rot_2 be the rotation matrix which transforms the $z(u_0, v_0)$ to the world frame for the final configuration of the robot.

The dot product of the initial and final normal vectors at the same point on the fingertip can be used to approximate $\Delta\theta$, the angle of rotation of the fingertip. The initial and final normal vectors are calculated from the equation for the z-vector of the contact frame. The z-axes vectors have already been normalized so the equation for the angle of rotation is:

$$\Delta\theta \approx \text{acos}\,(Rot_1 z\,(u_0, v_0) \bullet Rot_2 z\,(u_0, v_0)\,) \tag{34}$$

The effective axis of rotation for the entire probing motion may not be the same as the desired axis of rotation because the normal vector may twist as the probing motion moves along the surface. This would cause a slight error in the calculated angular rotation. Equation (34) gives us the magnitude of $\Delta\theta$, but the direction of rotation must also be known. Figure 15 shows how a negative rotation about the x-axis is calculated.

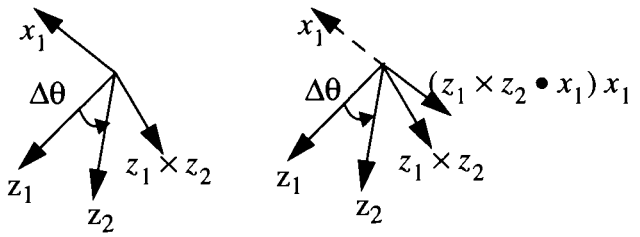

Fig. 15. Calculation of the angle of rotation

The sign of the rotation angle can be solved in the following manner:

$$\text{sgn}\,(\theta) \;=\; \text{sgn}\,(\,(z_1 \times z_2) \bullet x_1) \tag{35}$$

Simulation experiments were performed to analyze the sensitivity of EP1 for estimating curvature from rolling when error in the measurement of $\Delta\theta$ is present. The finger was rolled on spheres of various radii in simulation and the curvature of the spheres was estimated for various measurement errors of $\Delta\theta$.

The following parameters were used for the plots in figure 16:

Radii of spheres (R_2): 1000, 500, 50, 5, 1, 0.2, 0.05, 0.01, and 0.001 units

Angular rotations: 0.001, 0.01, 0.05, and 0.25 radians

Noise in $\Delta\theta$: 0, 0.0001, 0.0005, 0.001, 0.005, 0.01, and 0.05 radians

The same net angular rotation was used for all radii and errors. The noise term was added to the angular rotation of each of the eight probing motions in the direction of motion. The actual noise could be even larger than 0.05 radians (2.86 degrees), as most dexterous hands are tendon driven and are not extremely accurate in their position readings. If a rigid finger is used then the error will be determined by the accuracy of the robot model and the resolution of the joint encoders.

It can be observed from figure 16 that the curvature estimation error increases as the RCR increases and as the noise increases. It was also observed that as the length of Δs increased (related to increase in $\Delta\theta$), the error estimate became less sensitive to error. This result was expected since the error becomes a smaller percentage of the total angular rotation as Δs increases.

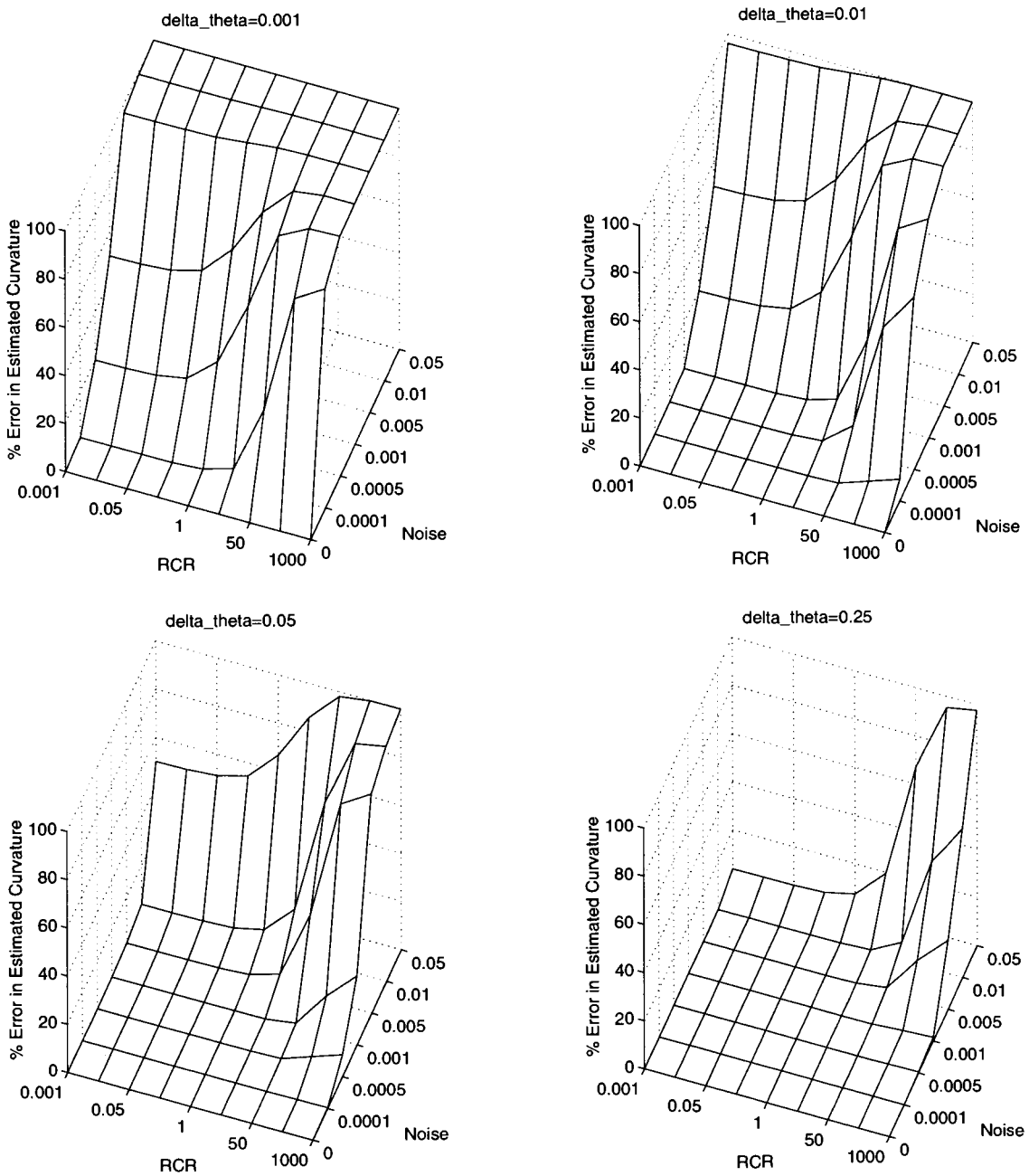

Fig. 16. Estimation error of sphere for $\Delta\theta$ values of 0.001, 0.01, 0.05 and 0.25

3.3.2 Objects with Varying Curvature

Increasing Δs can cause errors in surfaces with varying curvature. Montana's surface fitting method assumes that the surface has nearly constant curvature over the region being probed. If the probe travels far from the point of interest then the curvature may change considerably which will

cause error in the estimated curvature. For this reason, a paraboloid of revolution was investigated. The paraboloid was formed by rotating the curve $z = -Cx^2$ about the z-axis which produces the surface $z = -C(x^2 + y^2)$. The paraboloid surface is shown in figure 17 with a C value of 1.

The map for the paraboloid with parameter C is chosen to be:

$$f(u,v) = \begin{bmatrix} u \\ v \\ -C\left(u^2 + v^2\right) \end{bmatrix} \qquad \{ (u,v) \mid (-2 < u < 2, -2 < v < 2) \} \tag{36}$$

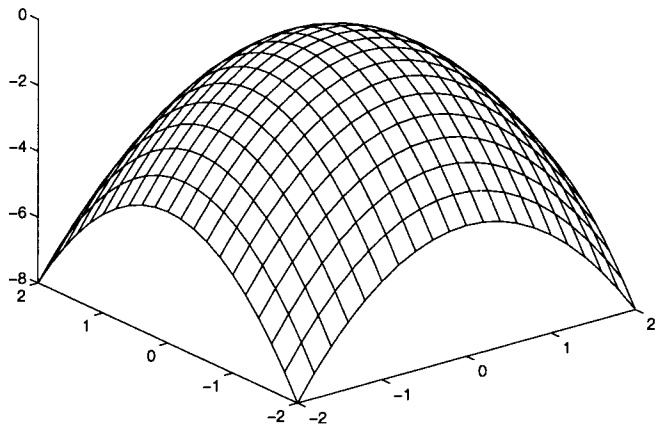

Fig. 17. Paraboloid surface for C equal to 1

The calculation of the Gauss map, Gauss frame, metric, curvature form, and torsion form for the paraboloid is provided in Appendix B.

The curvature form of the paraboloid is:

$$K_2 = \begin{bmatrix} \dfrac{2C}{\left(1 + (-2Cu)^2\right)^{\frac{3}{2}}\sqrt{1 + (-2Cv)^2}} & 0 \\ 0 & \dfrac{2C}{\sqrt{1 + (-2Cu)^2}\left(1 + (-2Cv)^2\right)^{\frac{3}{2}}} \end{bmatrix} \tag{37}$$

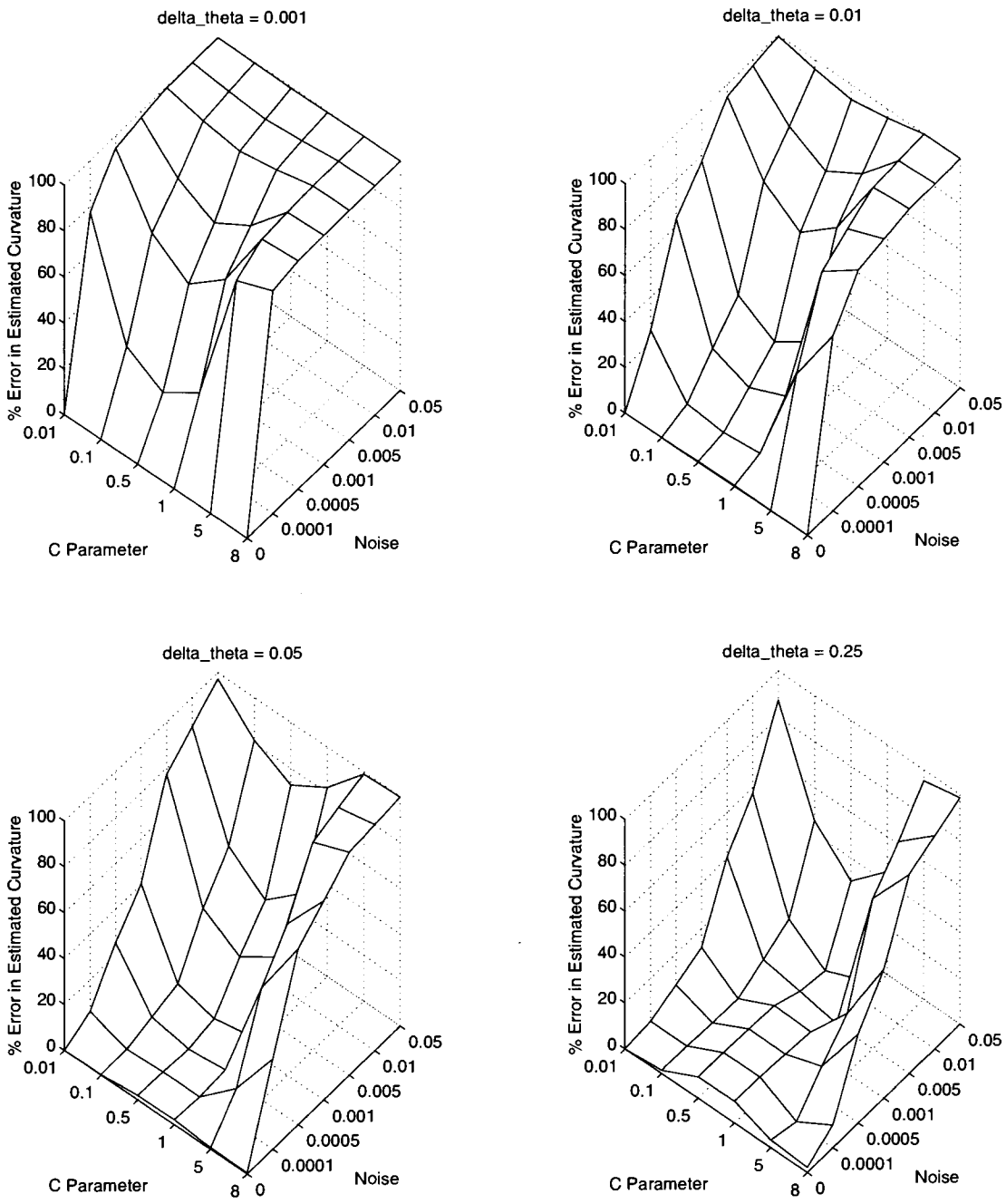

Fig. 18. Curvature estimation error in u direction of paraboloid. $\Delta\theta$ values: 0.001, 0.01, 0.05, 0.25

:Simulation experiments were performed to analyze the sensitivity of EP1 to changes in Δs for an object of varying curvature. The same fingertip radius as the previous simulations was used. The finger was rolled on paraboloids with various C values and the curvature at the point of interest

was estimated for various measurement errors of $\Delta\theta$. An initial (u, v) position of (1.0, 0.1) on the paraboloid was used. The curvature estimation will be affected by the arc length (Δs) of the probe because the curvature will increasingly change as Δs increases. The following parameters were used for the plots in figure 18.

Parameter C: 8, 5, 1, 0.5, 0.1, and 0.01 units

Errors added to $\Delta\theta$: 0.0001, 0.0005, 0.001, 0.005, 0.01, and 0.05 radians

These values for parameter C were chosen because they yield local radii of curvature between 2 and 500 units in the u direction. The curvatures in the u direction at (1.0, 0.1) for the selected values of C are shown in table 4.

Table 4: Radii of Curvature at (1.0, 0.1) for Values of C

C	8	5	1	0.5	0.1	0.01
u direction	485.8528	143.5480	5.7009	2.8425	5.3040	50.0301

It was found that the probing motions had to have a very small Δs *(less than 0.05 rad)* to accurately estimate the curvature at the point of interest for all values of C. The results of the simulations for various Δs values are shown in figure 18. Several trends can be observed in these graphs. The curvature estimate becomes inaccurate as Δs increases when there is no error present. The error directly due to Δs can be seen clearly in the graph of $\Delta\theta$ equal to 0.25 in figure 18, when the measurement error of $\Delta\theta$ is less than 0.0005 radians. If the error in the measurement of $\Delta\theta$ is large, it is best suppressed by a large Δs. When the error in the measurement of $\Delta\theta$ is small, there will be an optimal value of Δs which will be dependent on the rate of change of curvature near the point of interest, and the RCR.

Table 4 shows that the radius of curvature in the u direction varies from 485.85 at C equal to 8, down to 2.84 at C equal to 0.5, and back up to 50.03 at C equal to 0.01. As the measurement error of $\Delta\theta$ becomes large it can be seen from the previous graphs that the relative error in the curvature estimation increases as the RCR increases.

3.3.3 Tactile Sensor Resolution

The above simulations assumed an infinitely accurate contact sensor. This enabled us to determine the error caused by measurement error of $\Delta\theta$. The following section investigates the effect of sensor resolution. There are two possible types of sensors: discrete or continuous.

A discrete sensor is composed of very small sensor pads. In general, the sensor pad closest to the point of contact would be activated for a rigid probe. In the case of a soft contact, multiple pads may be activated and the centroid of the area would have to be found.

A continuous sensor would gave an accuracy with a Gaussian distribution of error. The accuracy of the sensor would be characterized by the standard deviation of the distribution.

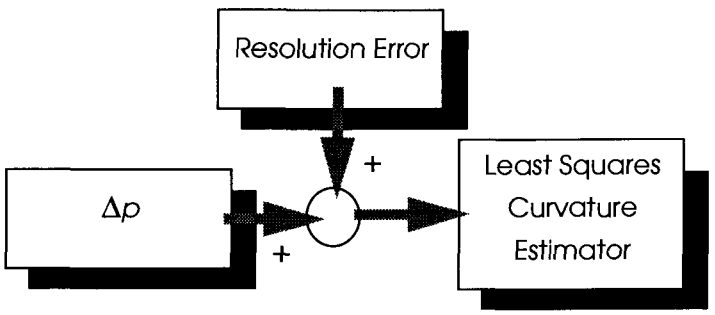

Fig. 19. Addition of sensor resolution error

In either case, the effect is that the measured change in contact position (Δp) will be slightly longer or shorter than the actual length of the change. A fingertip probe (R_1) of 1 unit radius was simulated to perform EP1 on spheres of various radii. The radii of the spheres (R_2) used in the simulation were: 1000, 500, 50, 5, 1, 0.2, 0.05, 0.01, and 0.001 units. The effect of sensor resolution error was determined for a tactile sensor with the following resolution errors: 0, 0.000001, 0.00001, 0.0001, 0.0005, 0.001, and 0.05 cm. These values were added to the final positions of each of the rolling probes in the direction of the rolling motion. The result of these simulation experiments is shown in the figure below. The error in estimated curvature was truncated at 100% to obtain a reasonable scale for the graphs.

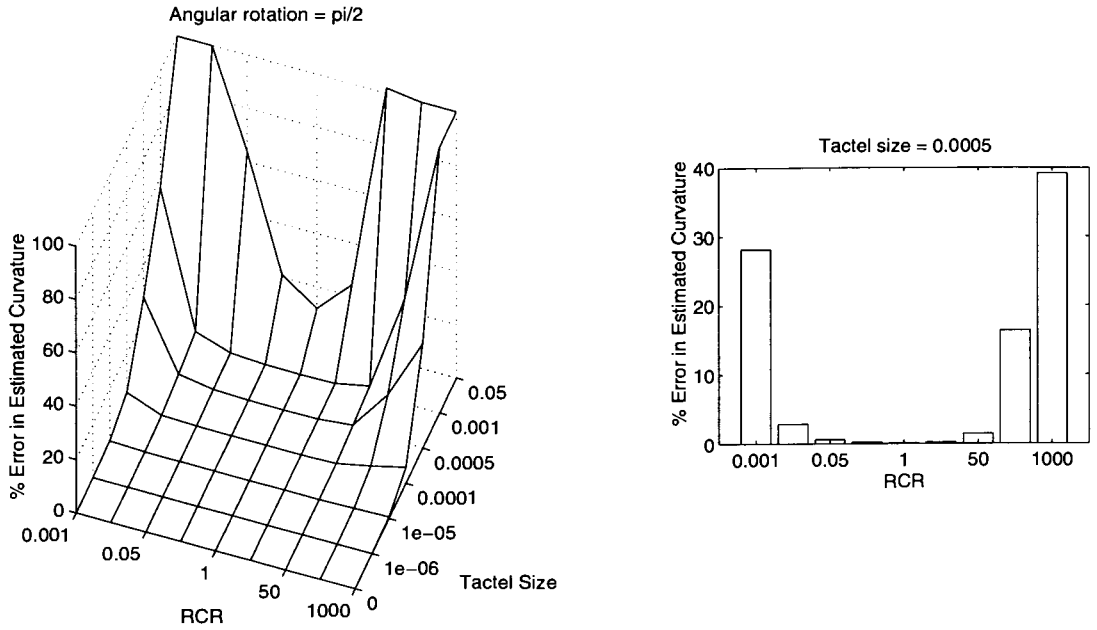

Fig. 20. Effects of sensor resolution

Several trends can be observed in the above graph. The curvature estimation becomes less accurate as the sensor resolution decreases. It was also found that the approach becomes more sensitive to sensor resolution as the RCR deviated from 1, i.e. if the curvature of the object is much greater or less than that of the probe, the error increased.

This latter trend was an unexpected result and further investigation was required to understand why this behavior was observed. The equation for Δs was solved for a 90 degree rotation ($\Delta\theta$) of the finger on spheres with RCR between 0.0001 and 25000. Figure 21 shows the reason for this trend. As the curvature of the object becomes very large (as in the case of an edge), Δs grows very small for a given $\Delta\theta$. In the extreme, Δs will grow smaller than the size of the elements of the tactile sensor and no Δp will be measured. As the RCR increases, the differential increase in Δs becomes very small. This leads to very large errors as the RCR becomes large. Therefore, it will be difficult to calculate the curvature accurately for very sharp and very flat objects. *Based on figure 21, it appears that a reasonable curvature estimate could be obtained with finite resolution for objects with a radius of curvature between 0.008 and 125.* This corresponds to an RCR between 125 and 0.008 (shown by the dashed lines in figure 21). The most accurate estimates will

occur when the object has a radius of 1 which corresponds with a RCR of 1.

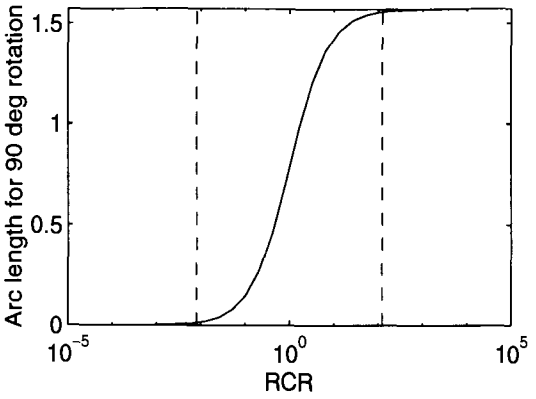

Fig. 21. Δs values for a $\Delta\theta$ of 90 degrees over a range RCRs

The results for many angular velocities and probing durations were simulated to investigate the combined effect of Δs and the resolution of the sensor. It was found that the accuracy of the estimate improves as Δs increases for a sphere. If Δs is very small and the resolution of the tactile sensor is coarse then the calculated Δp will either be zero or will be large because of a jump to the midpoint of the adjacent tactile array element. For objects of non-constant curvature, a satisfactory Δs will have to be determined which improves the estimate but is not overly affected by the changing curvature around the point of interest.

Resolution error is similar to the error obtained by using an insensitive probe and force/moment wrist sensor. A tactile sensor array would tend to round to the nearest tactile array element, while a force moment sensor would give a more Gaussian distribution of noise. Using a semi-spherical probe and a force/moment wrist sensor to determine contact position, Tsujimura and Yabuta [29] found their measurement error to vary 2.7 mm on average. From this they determined their tactile sensor system to be accurate to within 2.7 percent of the probe diameter. This would translate to an accuracy of 0.54 mm in our simulation study.

Based on figure 20, an estimate of the radius for spheres of radius 5 to 0.2 cm can be achieved with less than 25% relative error for a sensor accuracy of 0.5 mm using a $\Delta\theta$ *of* $\frac{\pi}{2}$ *rad.*

3.4 Summary of Results

The following section summarizes the results of the previous simulation experiments. Two sets of experiments were performed: infinite sensor resolution, and finite sensor resolution. The first section of the summary analyzes the results of the studies using infinite sensor resolution. The second section analyzes the results of the studies using finite sensor resolution.

3.4.1 Studies Using Infinite Sensor Resolution

The accuracy of the estimated curvature increases as Δs increases for an object with constant curvature. For surfaces of non-constant curvature, the accuracy of the estimated curvature decreases when there is no noise present. As the noise increases, the accuracy in curvature estimation can be improved by increasing Δs.

An explanation for the sensitivity to the RCR is as follows. Equation (24) was simplified by using a sphere of radius R_2 for the object and is shown in equation (38). As R_2 increases, the effect of the errors (e_x and e_y) also increase.

$$\dot{p}_1 = \begin{bmatrix} \dfrac{1}{\dfrac{R_1}{R_2}+1} & 0 \\ 0 & \dfrac{1}{\left(\dfrac{R_1}{R_2}+1\right)\cos(u_1)} \end{bmatrix} \begin{bmatrix} -\omega_y + e_y \\ \omega_x + e_x \end{bmatrix} \tag{38}$$

Figure 22 shows a summary of the trends found in the infinite sensor resolution experiments.

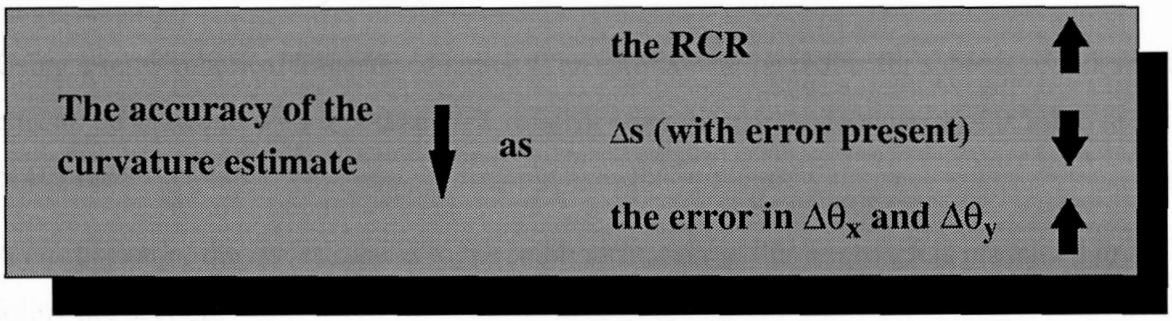

Fig. 22. Factors affecting curvature estimation for infinite sensor resolution

3.4.2 Studies Using Finite Sensor Resolution

Δs will have to increase to compensate for loss of accuracy due to the resolution of the sensor in order to get an accurate estimate of the curvature.

Figure 23 shows the trends in the accuracy of curvature estimation with finite sensor resolution.

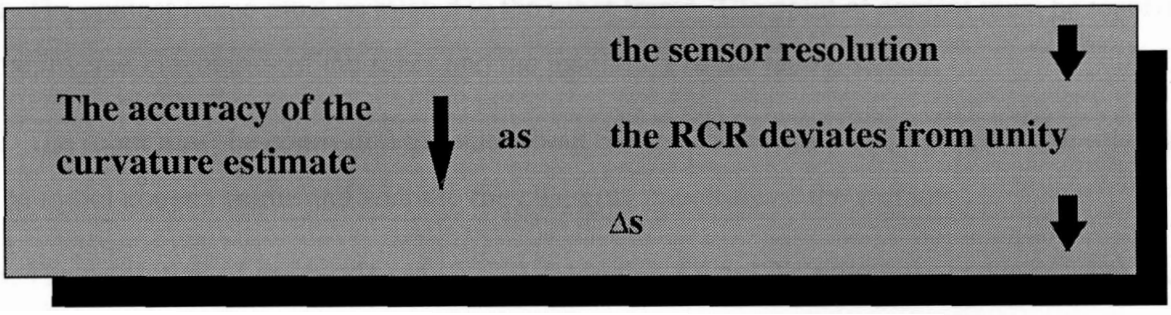

Fig. 23. Factors affecting curvature estimation for finite sensor resolution

3.5 Conclusions

Using Montana's method, it is practical to reasonably estimate the curvature of objects with a RCR between 0.008 and 125 units. This method is not suited for measuring the curvature of near planar surfaces or regions of high curvature unless the sensor is extremely accurate. The error due to sensor resolution is the limiting factor. Given the accuracy of the current sensor technology a relatively long Δs would be required to accurately measure surfaces of moderate curvature which

would reduce the accuracy of the curvature estimate.

Using a semi-spherical fingertip of radius 1, an estimate of the radius for spheres of radius 5 to 0.2 cm can be achieved with less than 25% relative error for a sensor accuracy of 0.5 mm using a $\Delta\theta$ of 0.5 rad.

A discussion of the issues related to the implementation of this approach is presented in the following section.

3.6 Implementation Issues

The physical implementation of this approach for determining curvature places many requirements on the experimental apparatus. Many calculations which were not required for the simulation studies will also have to be performed. In order to implement this approach the following things must be considered:

1. The contact frame must be related to the robot frame. The point of contact must be resolved by the inverse kinematics of the robot and the resolution of the tactile sensor.

2. The robot must be controlled to rotate about the instantaneous contact frame, or to rotate about the initial contact frame and adapt to the changing curvature of the surface.

3. The resolution of the tactile sensor will determine Δs and the minimum and maximum radii of curvature for the points on the surface of the object to be probed.

4. It will be difficult to determine whether the finger has maintained rolling contact or has slipped. The surface of the finger may require a special material to aid in slip prevention.

Chapter 4

EP2

High level information about the shape of an object can be gathered using multiple fingers of a dexterous robot hand. This chapter describes the second exploratory procedure (EP2) which gathers shape information over a patch on the surface of the object using a multi-finger sweep of the robot hand. The contact information can be used to recognize basic shape primitives, and potentially to recognize objects composed of these primitives.

The first section of this chapter provides an overview of EP2 which describes how it is used to extract shape information from the object. The following sections explain the procedure for fitting a B-spline curve to a set of data points and describes how to incorporate the normal information at these points. This curve fitting method is then extended to fitting B-spline surfaces to data and a novel method of incorporating the surface normal information is presented. The approach for shape analysis of the surface from the patch is presented along with a discussion of the factors which affect this analysis. The results of simulation experiments which test the ability of EP2 to recognize simple objects is also provided.

4.1 Overview

EP2 provides a method to generate an approximating surface of an object by sweeping a multifingered dexterous hand across the surface. The fingertips of the dexterous hand must be equipped with tactile or force/moment sensors which can be used to determine the coordinates of

the point of contact. The Gauss map of the finger tip is required to be known in order to determine the surface normal of the fingertip at the contact point. The geometry of the fingertips was chosen to be semi-spherical for simplicity. Figure 24 shows EP2 being performed on a cylinder rotated about the z-axis. The x and y axes are determined from the finger-to-finger, and sweep directions respectively as shown in figure 24.

The overall algorithm for analyzing a surface using EP2 is as follows:

1. Track the surface using three fingers of a dexterous hand and record the information required to determine the contact positions and surface normals.
2. Transform the data to a desired coordinate frame and scale for performing the surface fit.
3. Fit a B-spline surface to the data points using the surface normal information using either a tangent or position weighted fit.
4. Calculate the shape parameters on a discretized grid over the B-spline surface and calculate the mean and standard deviations of these parameters
5. Determine the best approximating shape based on the mean and standard deviation of the shape parameters.

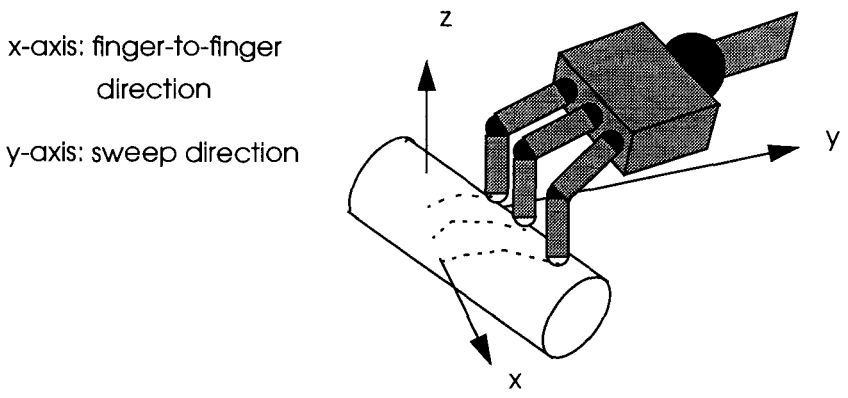

Fig. 24. The second exploratory procedure (EP2)

All dexterous hands have at least three fingers and three points of contact provides enough data for a reasonable approximation of simple surfaces. The surface fitting and analysis method could just as easily be applied for two contacts or for more than three contacts. In fact, one finger could be used to generate multiple lines or scattered data points which could be used to generate the

patch. A sweeping motion of three fingers is believed to generate sufficient data for fitting the surface using the least number of moves.

A B-spline surface patch is fit to the data obtained from EP2 which approximates the surface of the object. This enables the shape of the surface of the object to be analyzed using a small number of data points. A mathematical description of B-splines and the properties of their basis functions is provided in appendix A. A detailed understanding of B-splines will help the reader understand the remainder of this chapter.

A B-spline surface fit was chosen for its compact representation, and because the derivatives of the surface are easily obtained from this representation. Once the B-spline representation has been computed, it can be transformed to any new position by transforming the control points. In addition, B-splines can easily be composed of multiple order n segments which are all C^2 continuous. The following figure shows a cubic B-spline curve and B-spline surface and their defining control points.

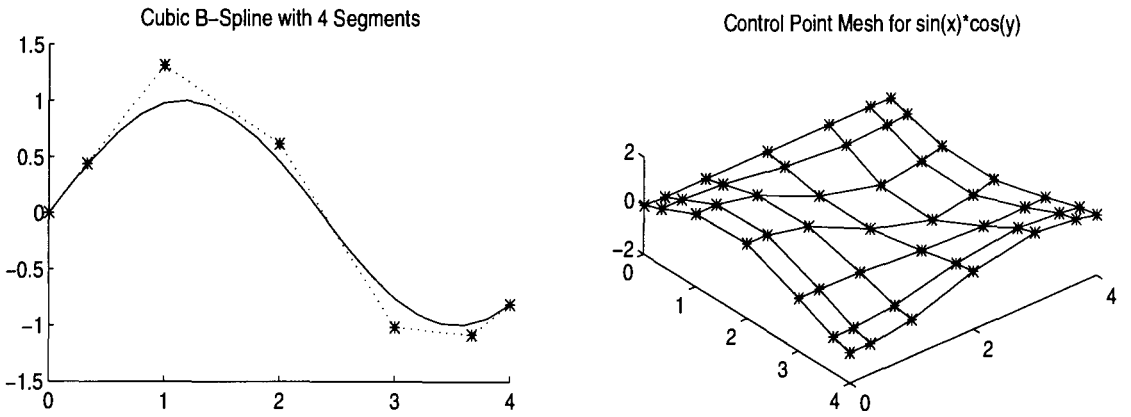

Fig. 25. Control points for a cubic B-spline curve and bicubic B-spline surface

A surface fitting technique was developed to incorporate the surface normal information at the contacts. The surface normals provide additional information which can be used to enable a higher order fit of the surface, and to reduce noise by facilitating a least squares approximation of the surface. This contribution will be described in detail later in this chapter.

In order to recognize the shape of the object, the surface curvature over the patch obtained by EP2

must be determined. The Gaussian and mean curvatures can be easily calculated from the B-spline representation of the surface. Shape properties will be determined from the Gaussian and mean curvatures over the patch. The shape properties of the patch can be computed from the Gaussian and mean curvatures as described in chapter 2. The shape properties of each point on the surface are invariant to scale and orientation.

4.2 Surface Generation from a Multifinger Probe

The primary motivation for incorporating the surface normal information into the surface fit was to provide additional constraints for the shape in the finger-to-finger direction. It is possible to exactly fit a quadric in this direction using three finger contacts; however, any noise will also be fit. A cubic or quartic fit is more desirable as a quadric fit is too restricted to approximate many shapes such as a saddle. A cubic fit requires a minimum of four equations to solve for the B-spline coefficients.

The density of the points in the sweep direction is arbitrary as the rate of sweeping can be set as desired. The surface normal will not add much more information unless the curve segment is not well approximated by a cubic in which case it may alter the shape of the fitted curve. As the number of points (or tangents) used to fit the curve increases there will be a decreasing effect on the fitted curve. If the surface being fitted is poorly approximated by the order of curve being used then more segments should be used in fitting the curve in the sweep direction. A fourth order curve could be used for curve fitting in the finger to finger direction. However, this could potentially fit a non-smooth curve to the data when only a few points are available. The appropriate orders of the tensor product surface used to fit the data will be determined by the shapes of the objects to be recognized and the noise present in the system.

In order to simplify the explanation of B-spline surface fitting, B-spline curve fitting will first be explained. This will be followed by an discussion of how to incorporate the tangent information into the curve fitting process. Finally a method for incorporating the surface normal information into the surface fitting process will be described.

4.3 2-D Curve Fitting with B-Splines

The feasibility of approximating the surface in the finger-to-finger direction can be investigated by a simple 2-D curve fitting problem. A 2-D quadric B-spline can be fit through the contacts obtained from three fingers of the dexterous hand. The quadric B-spline segment requires all three data points to satisfy the unknowns. A reader unfamiliar with basis splines (B-splines), their properties, and how they are computed is recommended to read appendix A before proceeding with this section.

The equation for a kth order B-spline with n basis functions is shown in equation 39. For a p segment spline, the number of basis functions is $k+p-1$.

$$S(x) = \sum_{i=1}^{n+1} c_i N_{i,k}(x) \qquad S(x) \Rightarrow (x, y) \tag{39}$$

where $N_{i,k}(x)$ are the values of the B-spline basis functions at x for the current set of knot vectors, and c_i are the *control points* which define the curve. The curve may be translated or rotated by transforming the control points. This is one of the primary benefits of the B-spline representation of a surface.

The x parameter is defined on the interval $[x_{min}, x_{max}]$. The spline is only defined in this interval. If a single, kth order spline segment was used, the knot vector would be composed of k values of x_{min} followed by k values of x_{max}. The spacing and number of the knots in the knot vector determine the basis functions over the interval. Figure 25 in section 4.1, shows a cubic B-spline with 7 control points, and uniform knot spacing. The knot vector for the curve is $\begin{bmatrix}0 & 0 & 0 & 0 & 1 & 2 & 3 & 4 & 4 & 4 & 4\end{bmatrix}$. Since only one 3rd order (quadric) segment is being fit, the knot vector for the spline would be:

$$\lambda = [x_{min}, x_{min}, x_{min}, x_{max}, x_{max}, x_{max}] \tag{40}$$

The linear system of equations for the B-spline curve is:

$$EC = Y$$

$$E = \begin{bmatrix} N_{1,k}(x_1) & \dots & N_{n,k}(x_1) \\ \dots & & \dots \\ N_{1,k}(x_g) & \dots & N_{n,k}(x_g) \end{bmatrix} \qquad C = \begin{bmatrix} c_{1x} & c_{1y} \\ \dots & \dots \\ c_{nx} & c_{ny} \end{bmatrix} \qquad Y = \begin{bmatrix} x_1 & y_1 \\ \dots & \dots \\ x_g & y_g \end{bmatrix} \tag{41}$$

where E is the observation matrix for the vector of x values of the data points, C is the matrix of control points, and Y is the vector of y values of the B-spline for the corresponding x values. The observation matrix has full column rank by nature of the basis functions.

The standard least squares formulation problem for g data points (x_r, y_r), requires minimization of the error (δ) according to the following equation:

$$\delta = \sum_{r=1}^{g} (w_r y_r - w_r S(x_r))^2 \tag{42}$$

where w_r is the weighting vector for the rth data point.

The weighted least squares solution of the control points can then be obtained by:

$$C = \left(E^T W E\right)^{-1} E^T W Y \tag{43}$$

where W is the matrix of weighting factors.

The following figure shows the analysis of a quadric B-spline curve fit. Three fingers are placed on a circular 2-D object of radius 7 at x equal to 0, 2, and 4 and the surface is approximated from these contacts.

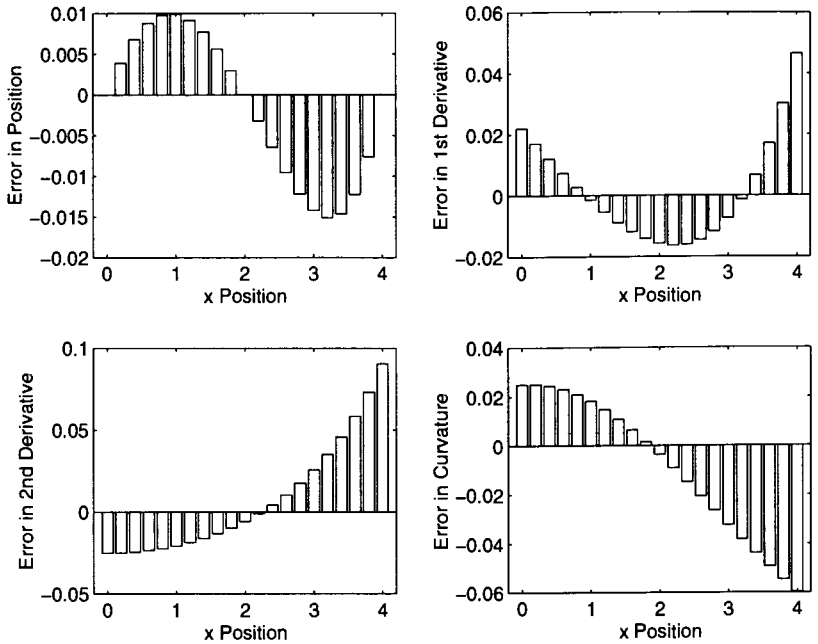

Fig. 26. Quadric B-Spline fit of a circular object

If more data points were available, a higher order curve could be fit to this data, or a least squares fit could be determined to reduce noise. The next section proposes a way to use the tangent information for this purpose.

4.4 2-D Curve Fitting with B-Splines Using Tangents

The tangent information can be used to supply additional information for fitting the curve. A quartic fit of the curve is now possible from only three finger contacts. Such a fit is over constrained by one and a least squares fit can be made. A least squares fit of a lower order curve can still be used if more data is available which will improve the accuracy of the fit.

For a quartic spline segment, the knot vector would be:

$$\lambda = [x_{min}, x_{min}, x_{min}, x_{min}, x_{min}, x_{max}, x_{max}, x_{max}, x_{max}, x_{max}] \tag{44}$$

The y values of the B-spline are calculated as before:

$$E_1 C = Y$$

$$E_1 = \begin{bmatrix} N_{1,k}(x_1) & \dots & N_{n,k}(x_1) \\ \dots & & \dots \\ N_{1,k}(x_g) & \dots & N_{n,k}(x_g) \end{bmatrix} \qquad C = \begin{bmatrix} c_{1x} & c_{1y} \\ \dots & \dots \\ c_{nx} & c_{ny} \end{bmatrix} \qquad Y = \begin{bmatrix} x_1 & y_1 \\ \dots & \dots \\ x_g & y_g \end{bmatrix} \tag{45}$$

The linear system for the tangents is:

$$E_2 C = T$$

$$E_2 = \begin{bmatrix} N'_{1,k}(x_1) & \dots & N'_{n,k}(x_1) \\ \dots & & \dots \\ N'_{1,k}(x_g) & \dots & N'_{n,k}(x_g) \end{bmatrix} \qquad T = \begin{bmatrix} 1 & T_1 \\ \dots & \dots \\ 1 & T_g \end{bmatrix} \tag{46}$$

where C is the same C as in equation 45, $N'_{i,k}(x)$ are the 1st derivatives of the basis functions at x, and T is the vector of tangents.

Given g data points (x_r, y_r), the least squares minimization function for the 2-D curve fit becomes:

$$\delta = \sum_{r=1}^{g} \left((w_{1_r} y_r - w_{1_r} S(x_r))^2 + (w_{2_r} y'_r - w_{2_r} S'(x_r))^2 \right) \tag{47}$$

The augmented system is then solved as before:

$$C = \left(\begin{bmatrix} E_1^T & E_2^T \end{bmatrix} \begin{bmatrix} W_1 & 0 \\ 0 & W_2 \end{bmatrix} \begin{bmatrix} E_1 \\ E_2 \end{bmatrix} \right)^{-1} \begin{bmatrix} E_1^T & E_2^T \end{bmatrix} \begin{bmatrix} W_1 & 0 \\ 0 & W_2 \end{bmatrix} \begin{bmatrix} Y \\ T \end{bmatrix} \tag{48}$$

The following graphs show the improvement in fit that can be achieved with the same number of finger contacts when the normal information is used. The same cylinder of radius 7, is touched by three fingers as before and a B-spline is fit through the contacts using the tangent information.

A quartic fit can now be achieved from the same three finger contacts. This provides a much better approximation to the position and derivatives and the error in curvature estimation becomes less than 0.03 units. In the plots for the position weighted curve (figure 27), the position error at the finger contacts (0, 2, 4) is nearly zero.

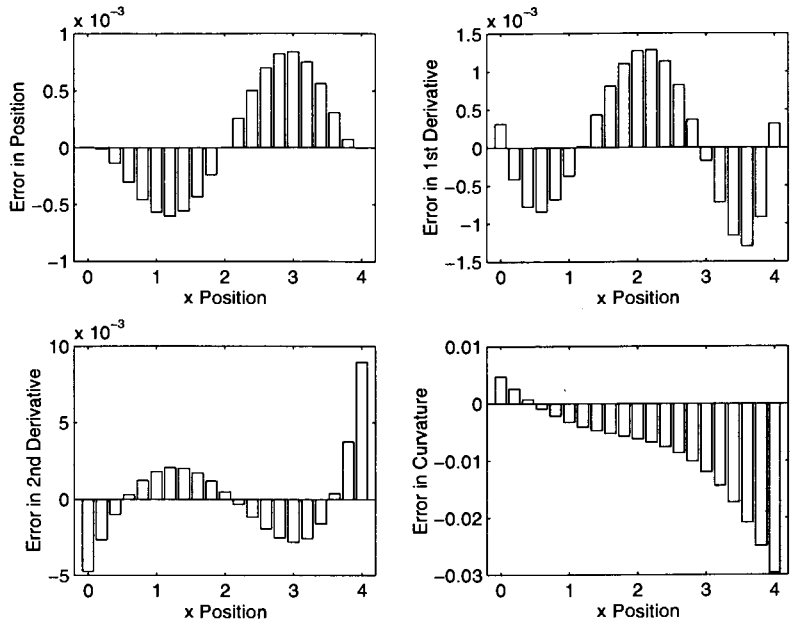

Fig. 27. Quartic fit (position weighted) of the circular object

The tangent weighted curve (figure 28) has nearly zero error in the first derivative at the finger contacts. However, it can be seen that the curvature estimate is not significantly affected by the weighing of tangent or position data. This is because the shape of the object is well approximated by the quartic fit.

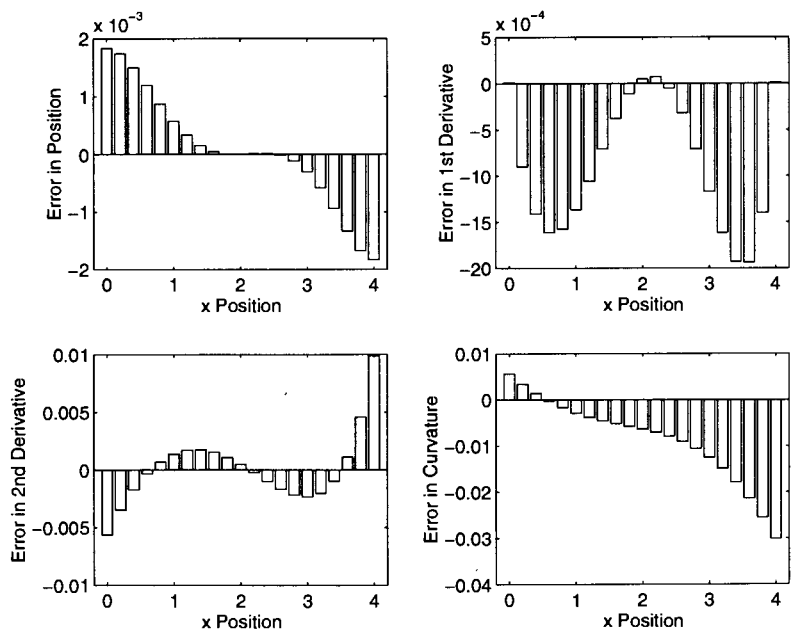

Fig. 28. Quartic fit (tangent weighted) of the circular object

4.4.1 Benefits from Using the Tangent Information

When the solution of a system is uniquely determined, any noise that is present in the system will also be approximated. An over determined system on the other hand can be solved using a least squares approach, which will have a smoothing or filtering effect. Using the tangents at the three contact points, a cubic fit of the control points changes from under determined to over determined.

Six equations are available for solving for the control points when the tangents are used which allows a least squares solution to be computed. The tangent information helps achieve the best compromise between the shape of the curve and actually passing through the points. When the tangent information is incorporated, the least squares fit of the surface is also a least squares fit for the derivative information as well. A good approximation of the derivative information is crucial when performing the curvature analysis of the surface.

4.5 Making Use of the Surface Normals

The number of contacts is fixed by the number of fingers however, there is additional data available for fitting the surface patch which until now has not been utilized by researchers in tactile sensing. The surface normal information at the contact point is available and can be used to provide additional data for approximating the surface.

The surface normal information is determined by the cross product of the derivative splines in the x and y directions. Therefore, the surface normal information cannot be directly used in the linear, least squares surface fitting algorithm. However, it is possible to include the derivative (tangent) information in the surface fitting algorithm. The tangent information in a desired direction on the surface can be directly obtained from the surface normal. The derivative in that direction is then determined from the tangent.

The derivative information supplies the additional constraints required to enable a cubic or quartic curve fit. It is also possible to weigh the fit toward the tangent or position data and to compensate for noise in the data.

4.5.1 Converting Surface Normals to Tangents

We formulate the surface fitting problem such that the derivatives of a B-spline use the same B-spline coefficients as the original spline. Using this approach the tangent information is easily incorporated into the least squares solution.

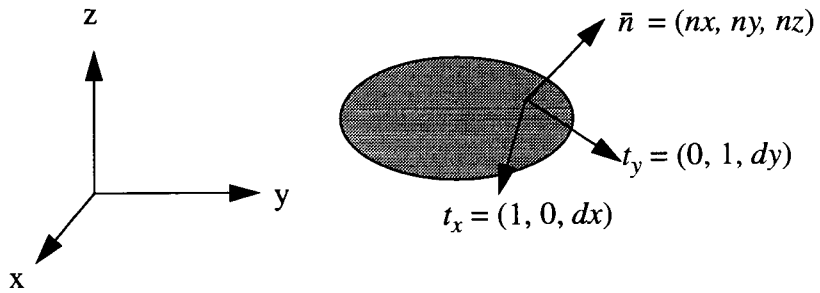

Fig. 29. Unit surface normal and tangents in x and y at a point on a surface

Let n be the surface normal and $\bar{n}$ be the unit normal. The tangents (to normal curves) in the x and y directions are related to the surface normal by the following equations:

$$\begin{aligned} t_x &= \begin{bmatrix} 1 & 0 & dx \end{bmatrix} \qquad n = t_x \times t_y = \begin{bmatrix} -dx & -dy & 1 \end{bmatrix} \\ t_y &= \begin{bmatrix} 0 & 1 & dy \end{bmatrix} \qquad \bar{n} = \begin{bmatrix} n_x & n_y & n_z \end{bmatrix} \end{aligned} \tag{49}$$

It can therefore be determined from the equations for the normal and the unit normal that:

$$-dx = \frac{n_x}{n_z} \qquad -dy = \frac{n_y}{n_z} \tag{50}$$

Let $P(x, y)$ be the bivariate spline fit for a patch of the surface of the object. The derivatives (tangents) in the x and y directions are determined from the surface normals using the following equations:

$$\frac{\partial}{\partial x} P(x, y) = \frac{-n_x}{n_z} \qquad \frac{\partial}{\partial y} P(x, y) = \frac{-n_y}{n_z} \tag{51}$$

The following section describes how the tangent information can be incorporated into the surface

fitting algorithm.

4.6 B-Spline Surface Fitting Using Surface Normals

The approach for incorporating the tangents can be extended from the previous 2-D example for 3-D surfaces. For surfaces, the tangent information is required in both the u and v directions of the surface. This information can be determined from the surface normal at the contact point.

The equation for a bivariate tensor product B-spline of order n in the x direction and order m in the y direction is:

$$S(x, y) = \sum_{i=1}^{n+1} \sum_{j=1}^{m+1} c_{i,j} N_{i,k}(x) M_{j,l}(y) \tag{52}$$

The basis function in x and y are denoted by $N_{i,k}(x)$ and $M_{j,k}(y)$ respectively. The basis function $N_{i,k}(x)$ is a function of x and not of an independent parameter t as is common in computer graphics. This is done to avoid error prone approximations using the arc length between points to estimate the parameter t. Similarly, $M_{j,k}(y)$ is a function of y and not of t. The arc length method is explained in detail in [25]. Basis functions in the x and y directions are independent. Therefore, the observation matrix for one bivariate patch can be written as the Kronecker product of the basis function in x and y:

$$E = N \otimes M \tag{53}$$

For g data points fit by a spline of order n in x and of order l in y, the N and M matrices become:

$$N = \begin{bmatrix} N_{1,k}(x_1) & \dots & N_{n+k,k}(x_1) \\ \dots & & \dots \\ N_{1,k}(x_g) & \dots & N_{n+k,k}(x_g) \end{bmatrix} \qquad M = \begin{bmatrix} M_{1,l}(y_1) & \dots & M_{m+l,l}(y_1) \\ \dots & & \dots \\ M_{1,l}(y_g) & \dots & M_{m+l,l}(y_g) \end{bmatrix} \tag{54}$$

This calculation is simplified if the data lies on a grid. For a p by q grid, there are only g/p unique values of x and g/q unique values of y. However, a sweeping motion of the fingers will generate scattered data so this simplification cannot be used.

The partial derivatives in the x and y directions must be calculated to incorporate the tangent information in the these directions. The tangents in the x and y directions can be obtained from the surface normals at the contacts. The E matrix for the single bivariate patch then becomes:

$$\begin{aligned} E1 &= N \otimes M \\ E2 &= N' \otimes M \\ E3 &= N \otimes M' \end{aligned} \qquad E = \begin{bmatrix} E1 \\ E2 \\ E3 \end{bmatrix} \tag{55}$$

The least squares minimization function becomes:

$$\delta = \sum_{r=1}^{g} \left((w_{1_r} z_r - w_{1_r} S(x_r, y_r))^2 + (w_{2_r} t_{x_r} - w_{2_r} S_x(x_r, y_r))^2 + (w_{3_r} t_{y_r} - w_{3_r} S_y(x_r, y_r))^2 \right) \tag{56}$$

where z_r is the z value of the rth data point, t_x is the tangent in the x direction, t_y is the tangent in the y direction, S_x is the partial derivative in x, and S_y is the partial derivative in y.

The tensor product B-spline coefficients are solved by:

$$C = \left(E^T \begin{bmatrix} W_1 & 0 & 0 \\ 0 & W_2 & 0 \\ 0 & 0 & W_3 \end{bmatrix} E \right)^{-1} E^T \begin{bmatrix} W_1 & 0 & 0 \\ 0 & W_2 & 0 \\ 0 & 0 & W_3 \end{bmatrix} \begin{bmatrix} Z \\ T_x \\ T_y \end{bmatrix} \tag{57}$$

where:

$$Z = \begin{bmatrix} x_1 & y_1 & z_1 \\ \cdots & \cdots & \cdots \\ x_g & y_g & z_g \end{bmatrix} \qquad T_x = \begin{bmatrix} 1 & 0 & t_{x1} \\ \cdots & \cdots & \cdots \\ 1 & 0 & t_{xg} \end{bmatrix} \qquad T_y = \begin{bmatrix} 0 & 1 & t_{y1} \\ \cdots & \cdots & \cdots \\ 0 & 1 & t_{yg} \end{bmatrix} \tag{58}$$

4.7 Other Considerations for Surface Fitting Using B-Splines

The above description of the method omitted many important details of the implementation of the surface fitting algorithm to simplify the presentation. These omissions are presented in this section for completeness. The reader is referred to Rogers and Adams [25] and Dierckx [12] for

more examples and a detailed discussion. This section describes how the knot vectors are selected, and how the control points for the B-spline surface are computed.

4.7.1 Knot Spacing

The spacing of the knot vectors must be selected before the basis functions can be calculated for a particular value. At present, only one bivariate spline segment is fit to the locus of points obtained by the multifinger sweep. This could potentially be increased in the future and was one of the reasons for the selection of B-splines.

If more than one spline segment was being fit in any direction of the spline (i.e. two bicubic segments in the y direction), the spacing of the knots would become important. Both Dierckx, and Rogers and Adams describe the effects of changing the knot spacing. Dierckx had developed a smoothing spline method which involves finding the optimum spacing of the knots. This will be discussed in greater detail in chapter 6.

4.7.2 Weighing Matrix

For n data points, the weighing matrix is a $3n$ x $3n$ diagonal matrix which enables the surface fit to best approximate the position or the tangents at each point. The first n diagonal elements are the weights of the position fitting equations, the second n diagonal elements are the weights of the x-tangent fitting equations, and the last n diagonal elements are the weights of the y-tangent fitting equations. The higher the relative weight, the more the corresponding equation will be weighted in the final fit.

Since the curvature is based only on the first and second derivatives at each point it is more important to approximate the tangents than the points at each point on the surface. This will be seen in the simulation results below.

4.8 Shape Description from Curvature

The shape properties of the sensed objects can be analyzed using the Gaussian and mean curvatures calculated at a grid of points over the patch. If the object is a single primitive then it

can be recognized from a single patch. If the object is composed of a combination of shape primitives then the individual primitives can first be recognized. The object can subsequently be determined from the adjacency graphs of the primitives for instance. The following experiments assume that the objects being probed are simple shape primitives.

4.8.1 Shape Analysis

The surface is sampled in an N x N grid, where N=4 for the following simulation, to facilitate quick analysis of the curvatures. The partial derivatives of the spline are calculated as:

$$S_x = (N' \otimes M)\, C \qquad S_y = (N \otimes M')\, C$$
$$S_{xx} = (N'' \otimes M)\, C \qquad S_{yy} = (N \otimes M'')\, C \qquad S_{xy} = (N' \otimes M')\, C \tag{59}$$

The minimum and maximum curvatures at the grid points are calculated using the equations described in chapter 2. Koenderink's shape parameters (*S, R, C*) are then calculated and used to determine the shape of the object. The shape of the sensed patch can be hypothesized by analyzing its *S, R,* and *C* parameters. The object can be recognized from this patch if the sensed region of the object is composed of only one of the basic shapes (flat, convex umbilic, convex cylinder, concave cylinder, or concave umbilic).

The expected values of *S* for each shape primitive is shown in chapter 2. A planar surface will have a nearly zero *R* value and a threshold of 1x10e-6 is used as the zero threshold. For planar surfaces, the S value is unimportant and likely inaccurate so in this case it is not calculated. The *C* value is $-\infty$ when *R* is equal to zero so the *C* parameter is also not calculated for planar surfaces.

4.8.2 Statistical Matching

The sixteen *S* values for the patch are computed over the 4 x 4 grid and are analyzed to find the mean and standard deviation. The mean is used to determine the shape and the standard deviation indicates the confidence of the match. The accuracy of the approach is measured by the standard deviation of the shape estimates for known shapes. The following section shows the simulation results for the shape matching of planes, convex and concave cylinders, and spheres.

4.9 Simulation Results for Determining Shape

The following simulation experiments test the accuracy of the estimation of S using the approach described above. It is assumed that the patch probed on the surface is only composed of one shape primitive. The following shapes were evaluated: plane, sphere, convex cylinder, concave cylinder, and plane. The approximating surfaces for each shape were determined for each parameter variation. In addition, surface approximations were calculated for a tangent weighted fit and a position weighted fit. A weighting factor of 100 was used for the favored data.

Each bar on the graphs below shows the estimated value of S and the standard deviation of S for the surface defined by a particular set of parameters. As described in previous sections, planes have a nearly zero value for R and are not concerned with the value of S.

4.9.1 Planes

Three planes of different steepness were tracked using EP2. The mean and variance of S over the patch was analyzed. The plane equations tested were $z=0$, $z=x+y$, and $z=3x+2y$.

All of these planes were successfully classified without error and the STD of R was negligible.

4.9.2 Cylinder

The first convex cylinder experiment used 3 radii and 7 rotations. This means that 3 x 7 x 2 = 42 surfaces were calculated including the tangent and position based fits. The mean S and standard deviation of S for the various convex cylinder surfaces are shown in the graph below. A bicubic B-spline surface is used to fit the data. The following radii and rotation angles for the cylinder were used:

Radii: 6, 10, and 500 units

Rotations: 0, 10, 30, 45, 60, 80, and 90 degrees

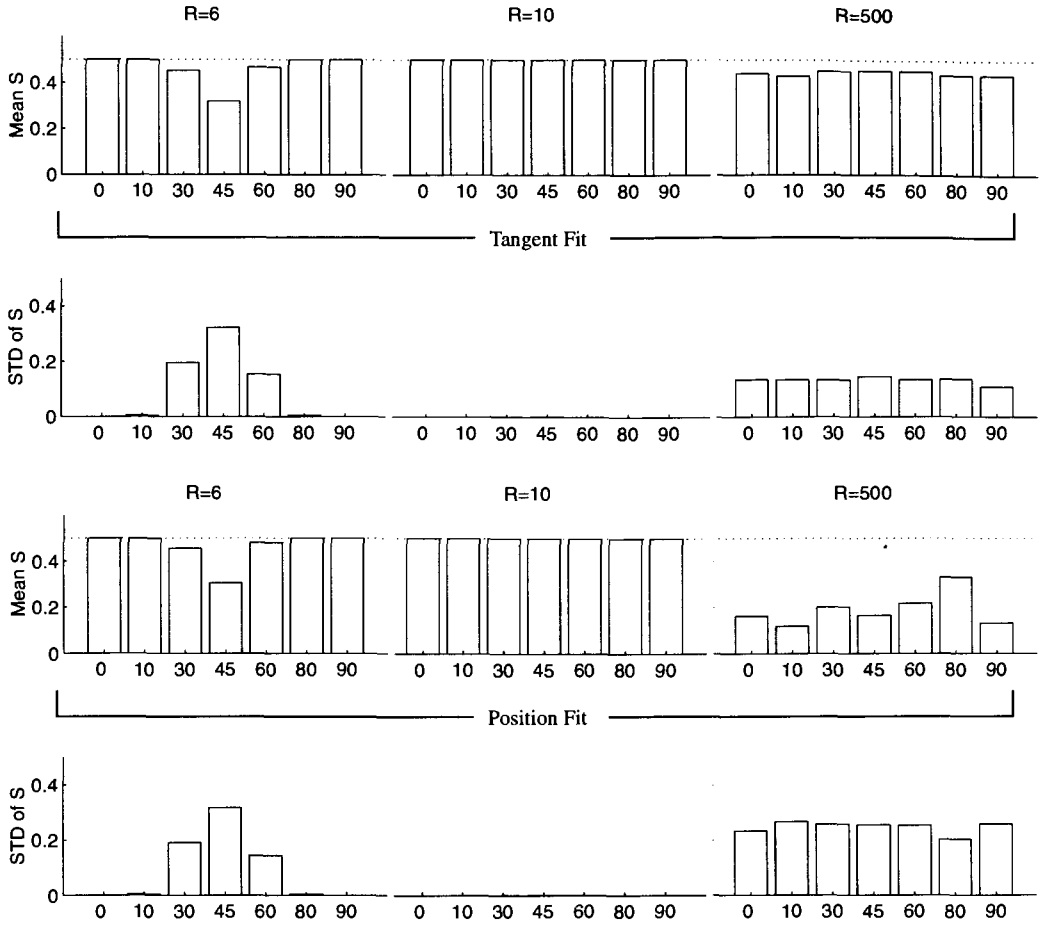

Fig. 30. Calculated mean S for and standard deviation (STD) of S for convex cylinders

In order to reduce the size of the plots and to facilitate easy comparison between plots, a condensed version of the above plot will be used throughout the remainder of this chapter. A condensed version of the data in figure 30 is shown in figure 31.

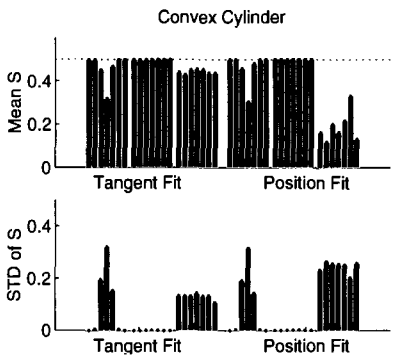

Fig. 31. Condensed plot of figure 30

The results of this experiment can be seen in figure 31 above. Cylinders of radius 10 are approximated very accurately using both tangent and position weighted fits. The approach is inaccurate for certain rotations of a cylinder of radius 6 for both position and tangent weighted fits. A satisfactory estimate of S is obtained for a cylinder of radius 500 using a tangent weighted fit. The position based fit is completely inaccurate for a cylinder of radius 500. The standard deviation of S is quite high when S is inaccurate so it is a good indicator of when the estimate of S is incorrect.

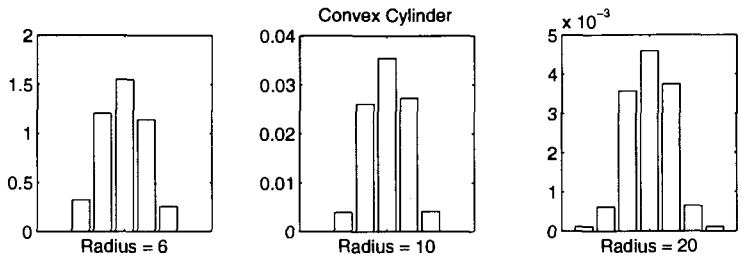

Fig. 32. RMS error in S for the rotations of three cylinders

Simulations were performed to analyze the effect of rotating the cylinder on the accuracy of the shape analysis. Cylinders of radius 6, 10 and 20 were rotated 0, 10, 30, 45, 60, 80, and 90 degrees and EP2 was simulated for each rotation. The root mean squared (RMS) error of the estimation of S for each rotation of each cylinder is shown in figure 32. The error in the estimation of S is highest for a rotation of 45 degrees. In this case the B-spline parameter directions are at 45 degrees to the principal directions of curvature of the cylinder. The error is minimal when the B-spline parameter directions are aligned with the principal direction of curvature. These directions are aligned for rotations of 0 and 90 degrees.

A third suite of experiments was performed to investigate the effect of the order of the fit and the radius of the cylinder on the accuracy of the estimate of S. The mean value and standard deviation of S were also calculated for a range of radii of cylinders. The range if radii used in the experiment was: 5.7, 6, 7, 8, 9, 10, 20, 40, 80, 150, 300, 500, and 1000. In order to obtain the worst case, the cylinders were rotated 45 degrees. The experiment was performed for biquadratic, bicubic, and biquartic B-spline surface fits. The results of these experiments are shown in figure

33 below. Accurate estimates of S were obtained for radii between 6 and 300 units. The tangent weighted fit was more accurate and had a smaller standard deviation for the large radii than the position weighted fit. The position data is sparse and is nearly linear. The tangent data causes the fit to more closely approximate the curvedness of the cylinder at the expense of inaccuracy in the position fit.

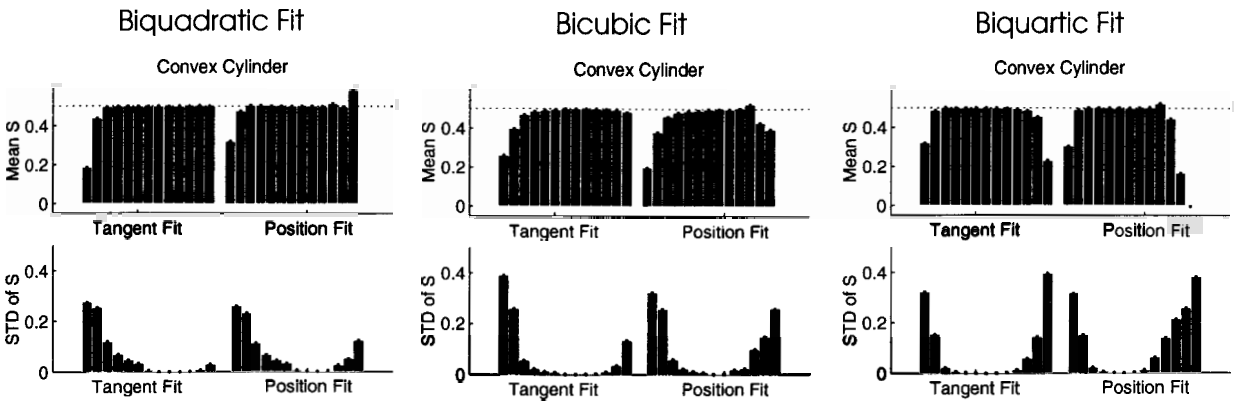

Fig. 33. Calculated mean S for and standard deviation (STD) of S over a range of radii

Identical results were obtained for a concave cylindrical section using the same experiments as above.

4.9.3 Sphere

Similar experiments were performed for three radii of spheres. The rotation of the sphere is not a factor because of its geometry. Biquadratic, bicubic and biquartic B-spline surfaces were fit for each of the radii listed below. The mean S and standard deviation of S for each of these surfaces was calculated and is shown in figure 34 below.

Radii: 5.7, 6, 7, 8, 9, 10, 20, 40, 80, 150, 300, 500, and 1000 units

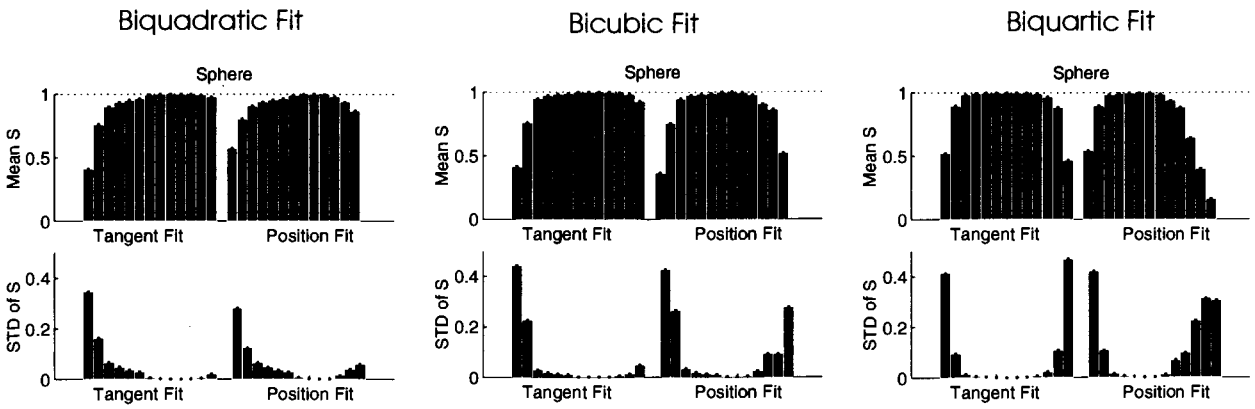

Fig. 34. Calculated mean S and standard deviation (STD) of S for spheres of various radii

As the order of the approximating surface increases, the accuracy of the estimate of S decreases for spheres with a large radius. As was the case with the cylinder, the tangent weighted fit is more accurate than the position weighted fit for spheres with a large radius. Otherwise, the tangent weighted fit is about as accurate as the position weighted fit. As the order of the approximating surface increases, the accuracy of the estimate of S increases. This surface fitting approach cannot successfully classify the sphere of radius 5.7, using either position or tangent fitting and a bivariate surface of order 5 (quartic) or less. The best estimates of S for spheres of large radius were obtained with a biquadratic surface fit. The standard deviation of S is quite high when the estimate of S is incorrect and is a good indication that the estimate is incorrect.

4.10 Summary of Results

Several experiments were performed to analyze the feasibility of using EP2 to obtain information about the shape of a surface and to recognize simple shape primitives. Koenderink's shape parameter (S) was used to provide shape information and the standard deviation of S was used as an indication of the accuracy of the estimate of S.

The accuracy of the estimate of S was affected by the following:

- The order of the approximation surface
- The angle between the directions of principal curvature of the surface and the parameter directions of the approximation surface

- The radius of curvature of the object
- Whether the approximating surface was tangent weighted or position weighted

Accurate estimates of S can be obtained for spheres, and convex and concave cylinders over a range of radii. Planar surfaces can also be easily recognized. Based on the these results, it should be straight forward to recognize these simple surfaces using this approach.

Experiments were performed to analyze the shape properties of a patch defined over the interval [0 4] in x and [0 4] in y. The B-spline surface patch was calculated based on the data obtained by EP2. The S value for cylinders and spheres of radius 7 to 1000 could be well approximated by a tangent weighted, biquadratic fit of the data obtained by EP2. The S value for spheres with a radius less than 10 were better approximated using a tangent weighted, biquartic approximating surface. However, a biquartic surface fit was less accurate for spheres with a radius greater than 300.

Tangent weighted fits gave a better approximation of S for spheres with large radius. This trend was more pronounced as the order of the approximating surface increased. When the object radius is large, position data is sparse and is nearly linear. The tangent data causes the fit to more closely approximate the curvedness of the object at the expense of inaccuracy in the position fit.

It was also observed that as the angle between the directions of principal curvature of the surface and the parameter directions of the approximation surface increase, the error in the approximation of S increased for cylinders with small radius. The maximum error occurred when this angle was 45 degrees. This is a problem with tensor product surfaces [26].

If the directions of principal curvature were computed, a second iteration of EP2 could be performed with the sweep directions aligned with one of the principal directions of curvature. If the radius of curvature is small, this approach would provide the greatest accuracy for estimating the shape of the surface.

Based on these experiments, the standard deviation of S is a good indicator of inaccuracy and reliability in the estimation of S. This information can be used as a measurement of the confidence of the classification of the shape of the surface.

Chapter 5

Experimental Results

Experiments were performed to test the effect of sensor noise on the approach for investigating shape. In order to obtain the data for three fingers of a dexterous robot hand performing EP2, a single probe made three passes of each surface. The probe has a circular end to simplify the calculation of the contact position and surface normal, and is mounted on a force/moment sensor. This sensor is attached to the 3 DOF robot as shown in figure 35. A discrete sampling of the surface was performed by the robot instead of tracking across the surface in order to simplify the control aspects of EP2.

The Experimental Robotics Lab (ERL) at SFU has a 3 DOF SCARA-Type robot named Freddy. A suite of high-level servo routines were developed to control the worm gear, wrist motor, and the links of Freddy to perform EP2.

A probe was designed to sample the surface of the object and mounted on the force/moment sensor. Using the force/moment sensor, the contact position and surface normal at the contact can be determined. This data was transformed to a new co-ordinate frame and then passed to the surface fitting software described in chapter 4. The B-spline surface was then analyzed to determine the shape of the object and to obtain qualitative information from the curvature properties of the surface.

A planar surface, convex cylinder, and concave cylinder were sampled by the robot and the results of these experiments is provided below.

5.1 Description of Experiment

In order to obtain the data which would be acquired by the three fingers of a dexterous robot hand performing EP2, a single probe made three passes of the surface. A discrete sampling of the surface was performed instead of tracking across the surface in order to simplify the control aspects of EP2.

Six points along the surface were probed with each finger. At each point, two data samples were taken to verify the integrity of the data. Therefore, a total of 36 data points were acquired for each surface. The joint angles of the robot and the x and y forces measured at the force sensor are taken for each data point. A sample is taken when the force sensor measures a force in the x - y plane with magnitude greater than 5 units. This magnitude of force was found to provide the best results while exerting a reasonable force on the object.

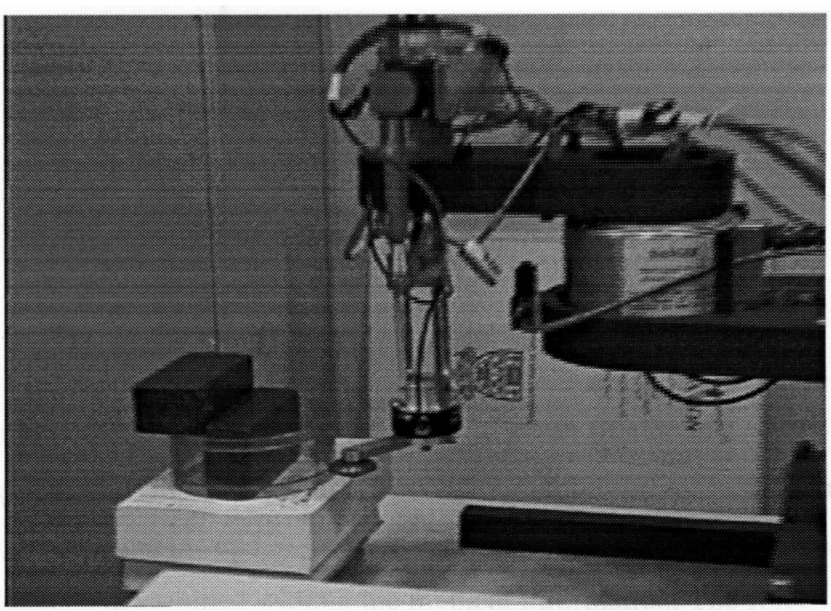

Fig. 35. Freddy sampling the planar surface

5.1.1 Determining the Contact Point and Surface Normal

The contact positions and surface normals were determined from the joint angles of the robot and the x and y forces. The direction of the applied force determines the contact position since the

direction of the force must be coincident with the surface normal at the contacting surface. Using the principle of transmissibility [5], the contact position on the probe can be resolved from the force measurements. The direction of applied force will be the same at the point of contact as the direction of the force measured at the force sensor.

If there is friction at the point of contact, the resultant force will not be normal to the surface of the object at the contact. The moment measured by the force/moment sensor will be required to determine the perpendicular distance to the line of applied force. The intersection of this line with the probe and the direction of the applied force determine the contact position on the probe. The surface normal is determined by the Gauss map of the probe at the contact point. Figure 36 shows the determination of the contact point on a rectangular probe. The origin of the force/moment sensor is located at the lower left corner of the probe in this example.

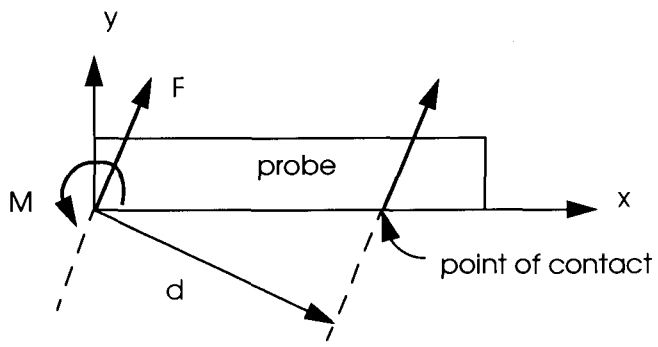

Fig. 36. Locating the point of contact on a bar shaped probe

A special probe was designed to sample the surface without friction in order to simplify the control of the sampling procedure and to facilitate tracking of the surface in the future. Since the friction force is negligible, and the end of the probe was designed to be circular, the contact point and surface normal can be determined without the moment information. The force measurement determines the direction of the surface normal. The contact position can be determined from the direction of force if the contact is on the spherical region of the probe as shown in figure 37.

The direction of the surface normal at an angle of θ about the center of the wheel of the probe is:

$$n(\theta) = (-\cos\theta, -\sin\theta) \tag{60}$$

Since the surface normal and applied force are co-linear, the direction of the surface normal can be found by:

$$\theta = \text{atan2}\,(fy, fx) \tag{61}$$

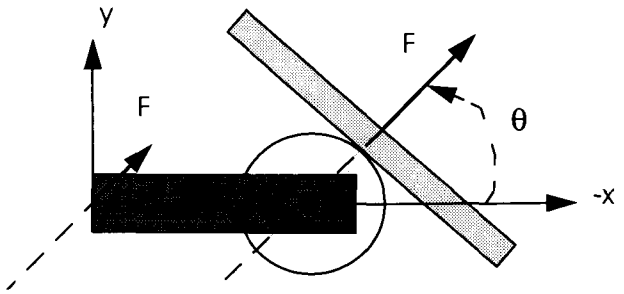

Fig. 37. Determining the contact on the new probe from the measured force

The z-component of the surface normal is assumed to zero initially to simplify the problem. This will give us a rough estimate of the magnitude of error in the estimated parameter. The probe was designed to determine the point of contact in the x-y plane only. The force in the z direction can be measured, but the geometry of the probe will not allow the contact position to be determined uniquely. A probe with a semi-spherical surface could be used for this purpose.

Once the contact point on the probe has been determined, the actual point of contact in the world frame must be determined from the joint angles of the robot. Figure 38 shows the parameters for the robot when the probe is attached. The lengths L_3 and L_4 are the length of the shaft of the probe and the radius of the wheel of the probe respectively.

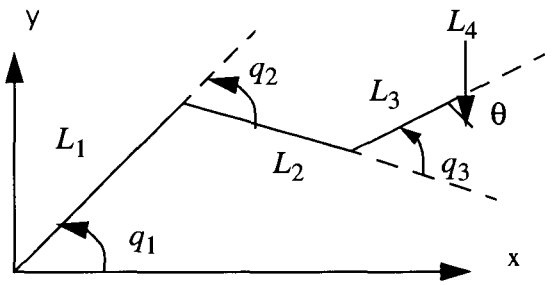

Fig. 38. The link lengths (L_i) and joint angles (q_i) for Freddy and the probe

The position of the point of contact in the world frame was determined from the joint angles of the robot, and the geometry of the probe using the following equations:

$$\begin{aligned} x &= L_1\cos(q_1) + L_2\cos(q_1+q_2) + L_3\cos(q_1+q_2+q_3) + L_4\cos(q_1+q_2+q_3+\theta) \\ y &= L_1\sin(q_1) + L_2\sin(q_1+q_2) + L_3\sin(q_1+q_2+q_3) + L_4\sin(q_1+q_2+q_3+\theta) \end{aligned} \tag{62}$$

The normal direction is obtained by finding the vector from the point of contact to the center of the circular part of the probe once these points have been transformed to the world frame.

5.1.2 Determining the Inside vs. Outside of the Surface

The surface fitting software expects the data to be in a particular orientation so that it can distinguish the inside of the surface from the outside of the surface. The direction of the surface normal of the fitted patch $S(x, y)$, is determined from the cross product of the derivatives of $S(x, y)$ in x and y.

$$n(x,y) = \frac{d}{dx}S(x,y) \times \frac{d}{dy}S(x,y) \tag{63}$$

The direction of the outward surface normal of the object is toward the finger contacting the object. The data obtained from EP2 is transformed from the robot end effector frame to a frame in which the normal has the proper orientation. The data points must be transformed to this frame of reference before the surface can be fit. Otherwise, a convex surface will be recognized as a concave surface and visa versa. The data was transformed such that the x direction was the finger-to-finger direction from right to left, the y direction was the direction of the sweeping motion, and the z direction pointed out from the surface of the object (see figure 24).

5.1.3 Limitations

There are several limitations to the present setup of the robot:

- The force sensor is accurate to 0.20 oz. in the x and y directions and to 0.40 oz. in the z direction [3].

- No documentation is available on the resolution of the optical encoders used on the robot. There are also errors in the model of the robot as some links are not perfectly rigid or straight.
- The wrist angle is fixed which limits the reachability of the robot.
- The probe was designed to measure the force in the x-y plane only. In order to find the surface normal of shapes which are curved in the z direction, a new probe is required.

5.2 Results

EP2 was performed on a planar surface, a convex cylindrical surface and a concave cylindrical surface. The contact points and surface normals were calculated for the data obtained for each of the surfaces. These were then transformed to a new co-ordinate system to be processed by the surface fitting software used in the simulations in chapter 4. The surface fit data is in centimeters.

The curvature properties of the surface are analyzed over an eight by eight grid. The mean value of S, standard deviation of S, mean value of R, and standard deviation of R are calculated for these points. The mean values and standard deviations of the principal curvatures are also calculated. The principal curvatures can be used to obtain quantitative information about the surface.

5.2.1 Planar Surface

A planar surface was placed in the workspace to be probed. The data was gathered from three sequential passes of the robot, representing each finger. The data was then transformed to the co-ordinate frame used by the surface fitting software. A B-spline surface was fit to the data and the curvature properties of the surface were calculated over an 8 x 8 grid.

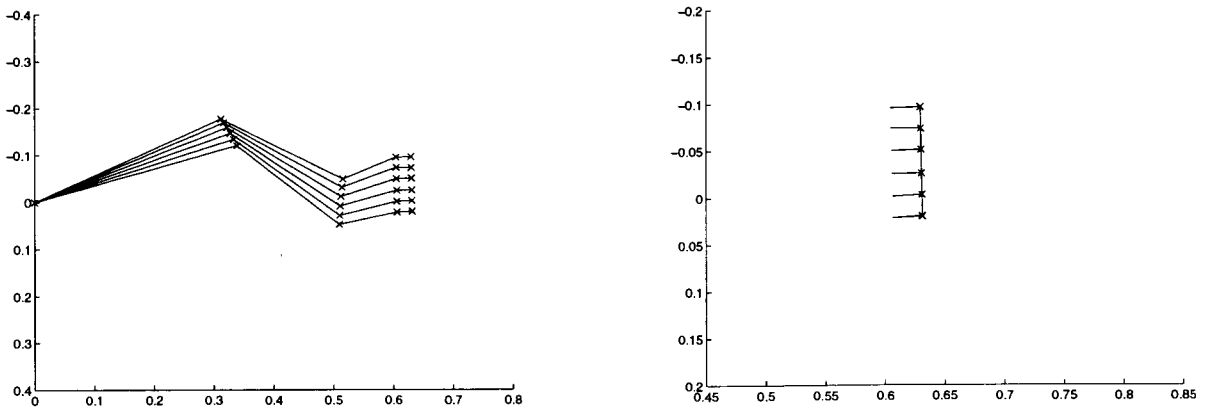

Fig. 39. Planar surface data for one finger: i) Configurations of the robot while sampling, ii) Contact points and surface normals

Figure 39 shows an example of the configurations of the robot while sampling with one finger across the planar surface.

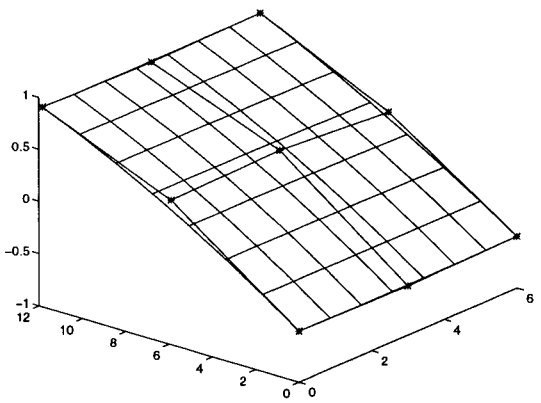

Fig. 40. Biquadratic fit of planar surface with its control point mesh superimposed

Figure 40 shows the biquadratic surface fit of the data and the control points of the surface. The control points should all lie in the same plane. It can be clearly seen that the surface is not perfectly planar from the lines of the control mesh.

An 8 x 8 grid of points on the surface was analyzed to determine the mean values of S and R and their standard deviations. The results are shown in table 5.

Table 5: Results of the Shape Analysis of the Planar Surface

	S	S.D. of S	R	S.D. of R
Tangent fit	0.4703	0.21204	0.004114	0.0006562
Position fit	0.3643	0.24721	0.003026	0.0009828

The expected value of R for a plane is zero. The mean value of R calculated from the surface was found to be very small, although significantly higher than for the simulation data. However, the standard deviation (S.D.) of R was very small which means that the surface is very uniform in its curvedness. The standard deviation of the S parameter is fairly high because the principal curvatures are nearly zero. If the R parameter were exactly zero (i.e. the principal curvatures were exactly zero) the S parameter would be undefined.

The noise in the data best suppressed by a biquadratic fit. The control point meshes for a bicubic and biquartic fit are shown in figure 41. The position weighed fits had a slightly different orientation but a similar error in the approximation of S. The approximations of S using higher order surfaces were much less accurate and had higher standard deviations.

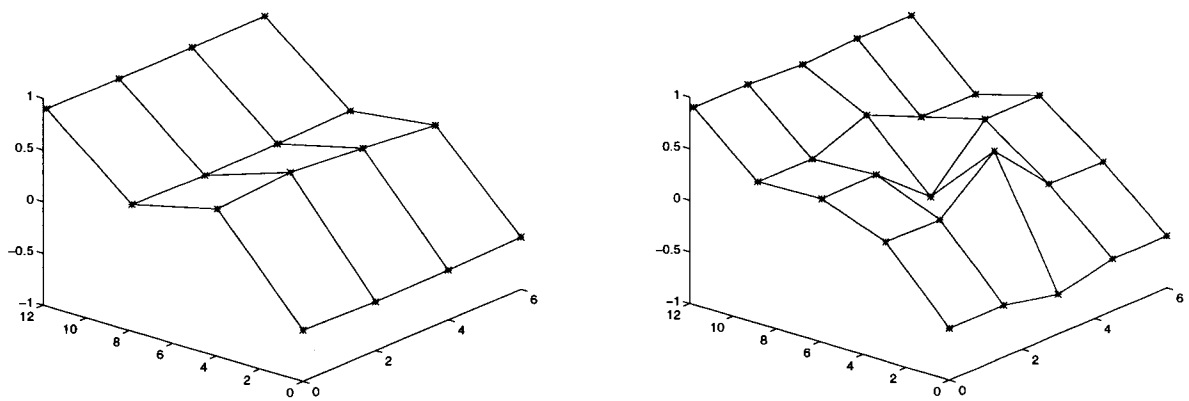

Fig. 41. Control meshes for: i) Bicubic fit of the data, ii) Biquartic fit of the data

5.2.2 Convex Cylindrical Surface

A convex cylindrical surface of radius 6.6 cm was placed in the workspace to be probed. The data was gathered as it was for the planar surface.

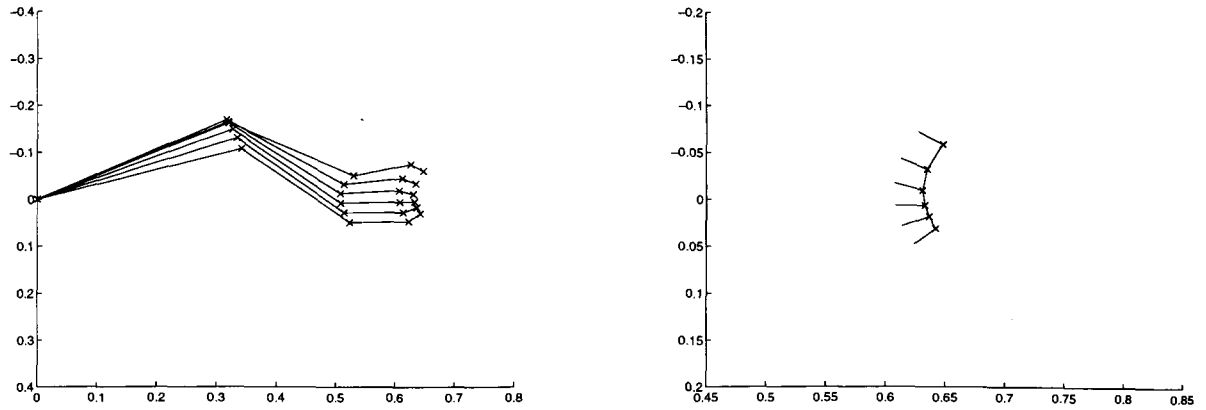

Fig. 42. Convex cylinder data for one finger: i) Configurations of the robot while sampling, ii) Contact points and surface normals

Figure 42 shows an example of the configurations of the robot while sampling with one finger across the planar surface.

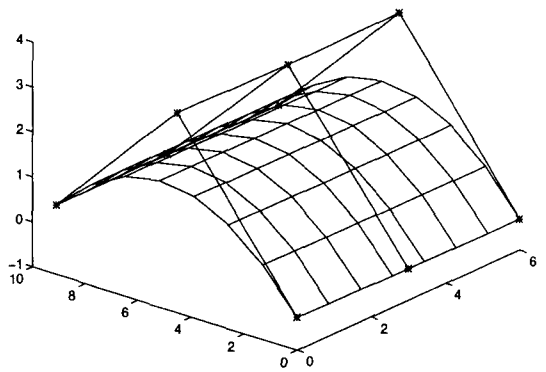

Fig. 43. Biquadratic fit of convex cylindrical surface with its control point mesh superimposed

Figure 43 shows the surface fit of the data and the control points of the surface. The control points form a convex hull of the surface as can be seen in the figure. If a higher order surface fit was used the control points would form a convex hull of the surface but it would not be minimal.

Once again, an 8 x 8 grid of points on the surface was analyzed to determine the mean values of S and R and their standard deviations. The results are shown in table 6.

Table 6: Results of the Shape Analysis of the Convex Cylindrical Surface

	S	S.D. of S	R	S.D. of R	Radius
Tangent fit	0.4980	0.009639	0.080290	0.024210	8.8078
Position fit	0.5014	0.015773	0.073446	0.016892	9.6304

The expected value of R for a cylinder of radius 6.6 is 0.1071. The mean value of R calculated from the surface was close to this value. The standard deviation (S.D.) of R was between 22 and 30 percent of the estimated value.

The expected value of S is 0.5 which is very close to the values estimated for the surface for both the tangent and position weighed fits. The S parameter of the tangent weighed fit has a standard deviation which is only slightly smaller than for the position weighed fit.

The estimated radius of the cylinder is more accurate for the tangent weighed fit. The accuracy of the quantitative characteristics of the surface is fairly low. The radius was measured within an accuracy of 1/3 of the actual radius.

The control point meshes for the tangent weighed bicubic and tangent weighed biquartic fit are shown in figure 44. The bicubic, tangent weighed fit shows one side of the surface to be flattened. The biquartic tangent weighed fit has the same general shape as the bicubic fit, although slightly more noisy.

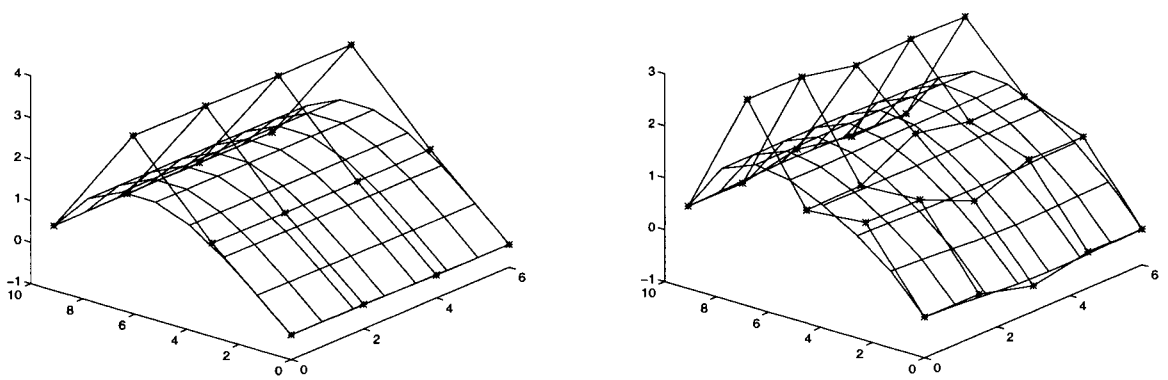

Fig. 44. Control meshes superimposed on the tangent weighed fits for: i) Bicubic fit of the data, ii) Biquartic fit of the data

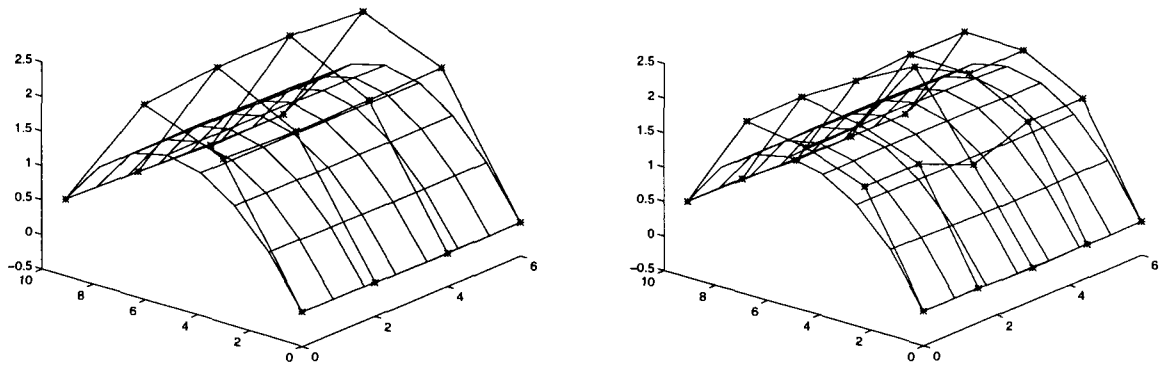

Fig. 45. Control meshes superimposed on the position weighed fits for: i) Bicubic fit of the data, ii) Biquartic fit of the data

The control point meshes for the tangent weighed bicubic and tangent weighed biquartic fit are shown in figure 45. The position weighed fits for the bicubic and biquartic surfaces provided a better approximation of the shape of the surface than the tangent weighed fits. This is due to the fact that the surface normal information is noisy and causes a greater error in the higher order tangent weighted fit than the position weighted fit. Both the bicubic and biquartic position weighted fits provided a good approximation of the surface.

5.2.3 Concave Cylindrical Surface

A concave cylindrical surface of diameter 22.5 cm was placed in the workspace to be probed. The data was gathered as for the previous surfaces. The middle finger (or middle sweep) did not make contact at one of the sample points. The two samples for this data point were ignored and only 34 data points instead of 64, were used to fit the surface.

Figure 46 shows an example of the configurations of the robot while sampling with one finger across the concave cylindrical surface.

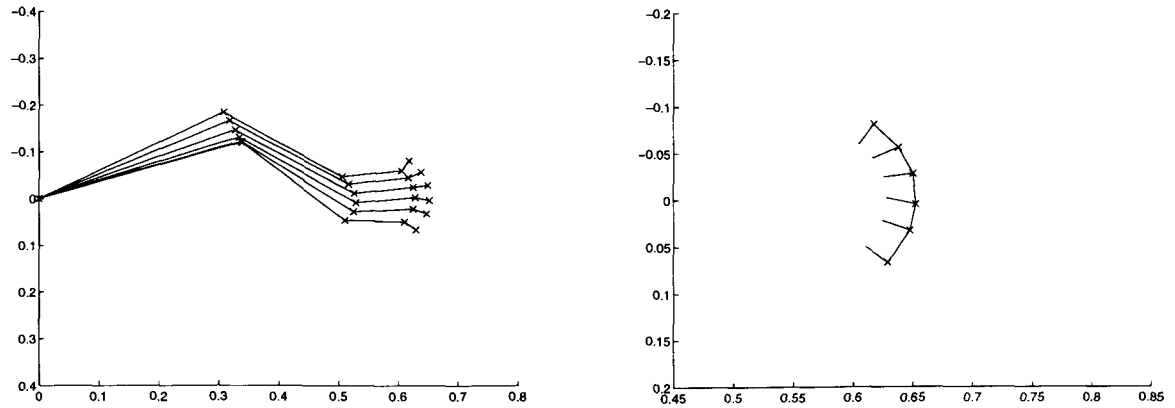

Fig. 46. Concave cylinder data for one finger: i) Configurations of the robot while sampling, ii) Contact points and surface normals

Figure 47 shows the surface fit of the data and the control points of the surface. The control points form a convex hull of the surface as they did for the convex cylinder.

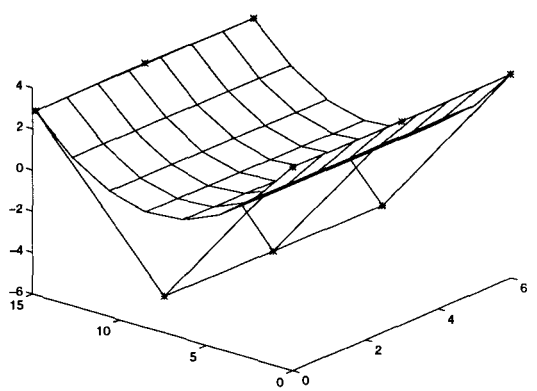

Fig. 47. Biquadratic fit of concave cylindrical surface with its control point mesh superimposed

Again, the grid of points on the surface was analyzed to determine the mean values of S and R and their standard deviations. The results are shown in table 7.

The expected value of R for a cylinder of radius 11.25 is 0.0629. The mean value of R calculated from the surface was close to this value. The standard deviation (S.D.) of R was between 28 and 44 percent of the estimated value.

Table 7: Results of the Shape Analysis of the Concave Cylindrical Surface

	S	S.D. of S	R	S.D. of R	Radius
Tangent fit	-0.4878	0.036813	0.057014	0.02732	12.4155
Position fit	-0.4483	0.123840	0.053336	0.01799	13.4831

The expected value of S is -0.5 which is close to the values estimated for the surface for both the tangent and position weighed fits. The S parameter of the position weighed fit has a much higher standard deviation than for the tangent weighed fit. The mean value of the S parameter for the tangent weighed fit is also slightly more accurate than for the position weighed fit.

The estimated radius of the cylinder is more accurate for the tangent weighed fit. The accuracy of the quantitative characteristics of the surface is once again fairly low. The radius was measured within an accuracy of 1/3 of the actual radius.

The control point meshes for the bicubic and biquartic tangent weighed fits are shown in figure 48. The bicubic, tangent weighed fit shows one side of the surface to be slightly flattened as in the previous section. The biquartic tangent weighed fit is much more noisy and provides a poor approximation.

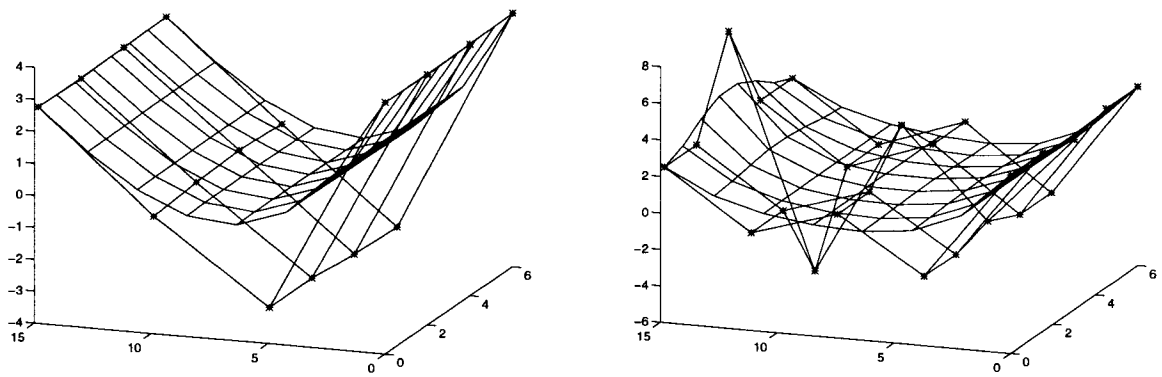

Fig. 48. Control meshes superimposed on the tangent weighed fits for: i) Bicubic fit of the data, ii) Biquartic fit of the data

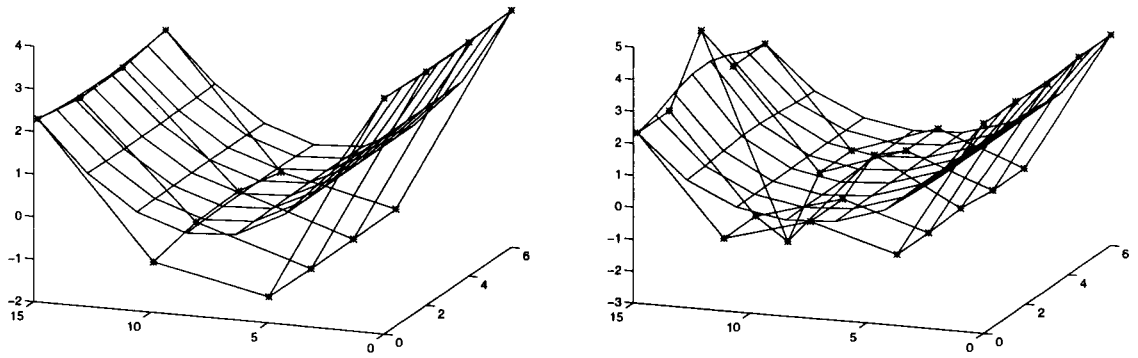

Fig. 49. Control meshes superimposed on the position weighed fits for: i) Bicubic fit of the data, ii) Biquartic fit of the data

The control point meshes for the tangent weighed bicubic and tangent weighed biquartic fit are shown in figure 49. The position weighed fits for the bicubic and biquartic surfaces provided a better approximation of the shape of the surface than the tangent weighed fits. Both the bicubic and biquartic position weighed fits provided a good approximation of the surface.

5.3 Conclusions

The proposed method for acquiring data using EP2 has been verified experimentally using a force/moment sensor to detect the contact position and surface normal. The method was capable of acquiring sufficiently accurate data enable the estimation of the shape parameters of the surface.

The biquadratic, tangent based fits provided the most accurate surface approximations for shape analysis. When higher order fits were used the position weighed fits were found to provide a more accurate surface representation.

The S parameter for the convex and concave cylinders could be estimated within 0.012 units of the actual value and with a standard deviation of less than 0.04 units for the concave cylinder. Even with coarse sensor resolution, we were able to obtain good results for qualitative shape recognition.

The planar surface was found to have a R parameter value which was an order of magnitude less

than the that of the cylindrical surfaces. A threshold must be determined for the value of R to distinguish planar surfaces. This threshold will depend on the accuracy of the data and the curvedness of the objects to be recognized.

If the object being sensed is a single primitive then the shape can be recognized from a small patch. If the object is composed of a combination of shape primitives, the individual primitives can first be recognized and then the object can be determined from the adjacency graphs of the primitives for instance.

Chapter 6

Discussion and Conclusions

6.1 Conclusions

A "blind man's paradigm" was used to test the extent to which tactile information can be used to describe the shape of objects with curved surfaces using two exploratory procedures. EP1 described a method to sense the shape of the object locally from rolling, and EP2 described a method to obtain shape information over a region of the surface of the object.

The simulation results for EP1 show that with finite sensor resolution, the method could potentially be used for an RCR between 0.008 and 125. The accuracy of the estimate of the curvatures will decrease as the RCR deviates from unity, and as Δs decreases except when the other errors are very small. When the other errors are very small, a long Δs will cause error for surfaces of varying curvature.

A second exploratory procedure (EP2) was described which is able to provide shape information over a region of the surface. A new method of incorporating the surface normal information into the B-spline surface fitting procedure was also presented. Using this method a patch could be fit to the data obtained by EP2. Koenderink's shape parameters were used to analyze the patch which allowed a confidence estimate of the shape classification to be calculated.

Using a patch defined over the interval [0 4] in x and [0 4] in y the following results were found.

The S value for cylinders and spheres of radius 7 to 1000 could be well approximated by a tangent weighted, biquadratic fit of the data obtained by EP2. The tangent information was useful for correcting the shape of the fit when the radius of the object was very large. Higher order fits provided a more accurate fit for objects with small radii but performed less well for objects with large radii.

The experiments performed with the SCARA-type robot confirm that simple shapes could be easily recognized using data collected by EP2. Tangent weighted biquadratic surface fits provided the best results. For surfaces of higher order, the position weighted fits produced a more accurate approximation of the surface. This was due to the fitting of the high order noise in the normal data by the tangent weighed fits.

6.2 Future Work

This thesis has laid the groundwork for future research into shape description and recognition of objects with curved surfaces using exploratory procedures. However, several requirements for the implementation of such a system have not yet been investigated. There are may unresolved issues relating to the control and planning requirements of EP1 and EP2. Many extensions can also be made to EP1 and EP2 to increase their ability to supply useful information about the shape of an object.

6.2.1 EP1

EP1 requires that the fingertip roll on the surface without slipping. This event must either be designed to be very unlikely (using high friction surfaces on the object and fingertip) or it must be able to be sensed. When slippage is detected during EP1 a recovery procedure is required.

A minimal force in the direction of the surface normal of at the contact point is required to be maintained while rolling on the surface during EP1. I have investigated the use of hybrid force control using a FSR pad as a tactile sensor. The force and position measurements of this sensor were coupled and the output of the sensor would drift over time. The use of this sensor is not recommended. More research is required to determine the best method to perform the control of EP1.

The curvature form for a point can be found using EP1, and provides the normal curvatures in the u and v directions. It would be useful to know the principal curvatures and their directions. If two iterations of EP1 were performed in two independent directions at a point. The information about the curvature in four directions at a point could be used to solve Euler's equation (64) for the principal curvatures (K_1 and K_2).

$$K(v) = K_1 \cos^2 v + K_2 \sin^2 v \tag{64}$$

The principal curvature information can be used recognize simple shapes and the directions of the principal curvatures can be used to determine the orientation of certain objects.

6.2.2 EP2

All the links of each finger and the supporting robot must be controlled during EP2. A small force to activate the sensors must be maintained while tracking across the surface. Also, the degrees of freedom of the system is very large and a unique set of joint angles will not exist. The fingers must be maintained a certain distance apart during the tracking motion of EP2. It is unknown whether a tracking motion in which the interfinger distance decreases during the sweep is useful. I have found that humans seem to use this approach when tracking the surface of an object. An investigation of the effect of varying the interfinger distance is required.

There are several unsolved planning requirements for the implementation and progression EP2. The system will require task planning decisions to be made based on the objectives and the acquired knowledge. Motion planning issues for collision detection, configuration of the hand and path planning for EP2 must also be solved.

A recovery procedure is required when one of the fingers loses contact during EP2. This may be due to a hole in the surface, or due to a sudden change in the surface normal such as at the intersection of two faces on a cube. If the intersection between two planar surfaces is reached, a discontinuity must be inserted into the surface fit. This can be accomplished by the selection of the knot vector used to generate the control points of the approximating surface. Alternatively, if a discontinuity is detected, the EP could be abandoned and a new EP could be performed for each side of the discontinuity. Edge information can be quite useful in recognizing complex objects. If

a discontinuity is detected, a single finger could perform an edge-following EP [24] to trace out its extent and shape.

The information gathered about the curvature over a patch can be used as a source of knowledge for future probes. An estimate of the curvature flow over the patch could be determined by finding the directions of principal curvature at the sample points. This information could be used to plan surface explorations in the directions of the curvature flows using EP2. It could also provide orientation information for cylindrical objects.

In the same way that Roberts [24] used an interpretation tree for selecting the best active sensing move, an interpretation tree could be built based on the acquired shape properties of the object to guide future probes.

6.2.3 Surface Analysis

The criteria for the characterization of patches is that they must be: discriminatory, and represented in a compact fashion. Once a patch has been probed, the data obtained may be insufficient to determine the object and the next probe may be guided by the curvature flow, or the adjacency relations of the features of the feasible matches.

There are many different methods that can be used to generate the approximating B-spline surface. These include multi-segment fits, dynamic knot placement, using a smoothing spline fit, and boundary trimming.

Only one B-Spline patch is presently used to define the approximating surface patch. If more knots were used in the knot vector, a multi-segment fit of the data would be performed. These knots could be uniformly spaced but that would limit the accuracy of the approximation for a given number of segments. Dynamic placement of the additional knots would provide an optimal fit of the data. This is a non-linear problem and has been addressed by Dierckx in [12]. A similar approach could be used to perform dynamic knot placement for the surface fitting algorithm defined in this thesis.

Dierckx [12] has defined a smoothing spline which uses a smoothing parameter to set the desired level of detail of the surface fit. He has developed a software package of fortran routines called

FITPACK (available by ftp) to perform various surface and curve fitting algorithms. His implementation calculates the derivatives of the B-spline surface by differentiating the matrix of control points. This does not facilitate the inclusion of the tangent information when determining the control points. A new implementation of derivative calculations could be made using the equations defined in Appendix A of this thesis. This would enable the tangent information to be used to calculate the control points of Dierckx smoothing spline.

If the interfinger distance changes or the sweep direction curves during EP2, the boundary of the patch will not correspond to the boundary of the region explored by EP2. A trimming curve can be defined for the surface which will show the patch over the region tracked by EP2. There are several sources of information on defining trimming curves including [14] and [17].

6.2.4 Analysis of Patches with Varying *S*

Many surfaces will not be composed of simple planar, cylindrical, or spherical regions with uniform values of *S*. If these surfaces are sufficiently smooth, they will have planar, convex, concave, and saddle regions which can be grouped by a mean and spread of *S*. These regions can be used as features of the surface and can be used for recognizing and orienting the surface. Such a description would allow scale independent models to be used. An example is shown below for a saddle surface.

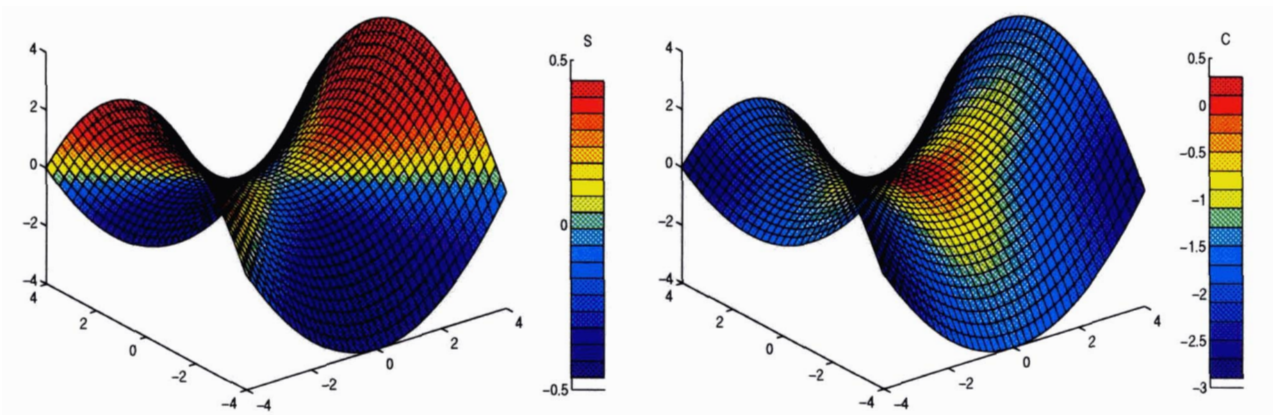

Fig. 50. A saddle with the values of *S* (left) and *C* (right) mapped onto its surface

The saddle has many regions with similar values of S and C as seen in figure 50 above. These regions are features of this saddle which are independent of the scale of the surface. A saddle twice the size would have the same values of S at the corresponding points. This representation has advantages over previous region maps based on the signs of the Gaussian and mean curvatures. Any value of S can be used for the mean of a region and the region can represent any specified range of S. When small ranges are used for each region, the surface description is more quantitative.

6.2.5 Multiple Shape Primitives in a Patch

The next step in recognizing more complex objects will be to process patches composed of multiple primitive shapes. The region being probed may contain the junction between two surface primitives. An example object would be a cylinder with semi-sphere caps at either end. The patch must be analyzed using a finer grid and a region map of the various shape primitives can be made. A minimum region size would be imposed to prevent the patches from being too broken.

If a long sweeping motion was performed, it may track over a discontinuity that will cause a large error in the approximating surface. It may be possible to sense the discontinuity at the time of tracking if sequential surface normals differ by more than a specified angle in the sweeping direction. Discontinuities in the patch can be accommodated by repeated knots in the defining knot vectors for the surface. Ideally, these discontinuities would cause repeated knot values to be computed in a dynamic knot placement scheme.

Appendix A - B-spline Surfaces

The following mathematical background provides an introduction to B-splines and B-spline tensor product surfaces, the basis functions, and the properties of these functions.

A.1 B-Splines

The equation for a B-spline of order k (degree k-1) is:

$$S(x) = \sum_{i=1}^{n+1} c_i N_{i,k}(x) \qquad x \in [\lambda_0, \lambda_{k+n}) \qquad 2 \le k \le n+1 \tag{65}$$

where n+1 is the number of basis functions and $N_{i,k}$(x) are the basis functions. See the section below for an explanation of the basis functions. The c_i's are the B-spline coefficients which define the control points.

A.1.1 Knot Vectors

The interval $[\lambda_0, \lambda_{k+n})$ is divided up into k+n subintervals by a knot vector. The knot values λ_i do not have to have uniform spacing but they must satisfy the relation $\lambda_i \le \lambda_{i+1}$. The number of knot values and their spacing will affect the basis functions for the interval. Rogers and Adams [25] shows examples of the basis functions using different knot vectors over the interval [0, 3].

The number of knot values in the knot vector is k+n+1. Thus, for a cubic spline (k = 4) the minimum number of knot values required is 8 since the minimum for n in equation (65) is k-1. A Bezier spline representation can be obtained by duplicating the knots at the beginning and end of a spline segment k times.

Thus the knot vector [0, 0, 0, 0, 4, 4, 4, 4] would give the Bezier spline basis functions (also known as Bernstein basis functions) over the interval [0, 4].

A.1.2 Normalized Basis Functions

Consider the function $g(t) = (t-x)_+^{k-1}$ which is defined as being nonzero only when $(t-x) > 0$. The basis functions are based on the divided difference of this function.

The *k*th divided difference of the function f is defined as follows:

$$[\tau_i, \ldots, \tau_{i+k}]f = \frac{[\tau_{i+1}, \ldots, \tau_{i+k}]f - [\tau_i, \ldots, \tau_{i+k-1}]f}{\tau_{i+k} - \tau_i}, \text{ if } \tau_i < \tau_{i+k} \qquad (66)$$

$$[\tau_i]f = f(\tau_i)$$

$$[\tau_i]f = f(\tau_i), \text{ if } \tau_i = \ldots = \tau_{i+k} \qquad (67)$$

The normalized B-spline basis function of order k and with knots $(\lambda_0, \ldots, \lambda_{k+n})$ is defined as the *k*th divided difference of *g*:

$$N_{i,k}(x) = (\lambda_{i+k} - \lambda_i)\,([\lambda_i, \ldots, \lambda_{i+k}]\,g(t)) \qquad (68)$$

There are *k* normalized B-splines which contribute to the approximation over the desired range assuming there are *k*-1 knots before or equal to the beginning of this range and *k*-1 knots after or equal to the end of this range.

This equation can be calculated using the following recursive formula:

$$N_{i,k}(x) = \frac{x - \lambda_i}{\lambda_{i+k-1} - \lambda_i} N_{i,k-1}(x) + \frac{\lambda_{i+k} - x}{\lambda_{i+k} - \lambda_{i+1}} N_{i+1,k-1}(x) \qquad (69)$$

$$N_{i,1}(x) = \begin{cases} 1, & \text{if } x \in [\lambda_i, \lambda_{i+1}) \\ 0, & \text{if } x \notin [\lambda_i, \lambda_{i+1}) \end{cases} \qquad (70)$$

The basis functions for a B-spline with uniform knot spacing is shown in the figure below. The knot vector used for this 4th order B-spline is [0 0 0 0 1 2 3 3 3 3]. The curve is composed of three, 4th order segments as described by the formula above. Four of the six basis functions will be used to define each of the three spline segments. For the first segment, $N_{1,4}$, $N_{2,4}$, $N_{3,4}$, and $N_{4,4}$ are active. This can be seen in the graph below as these are the only basis finctions with non-

zero values in the range [0, 1].

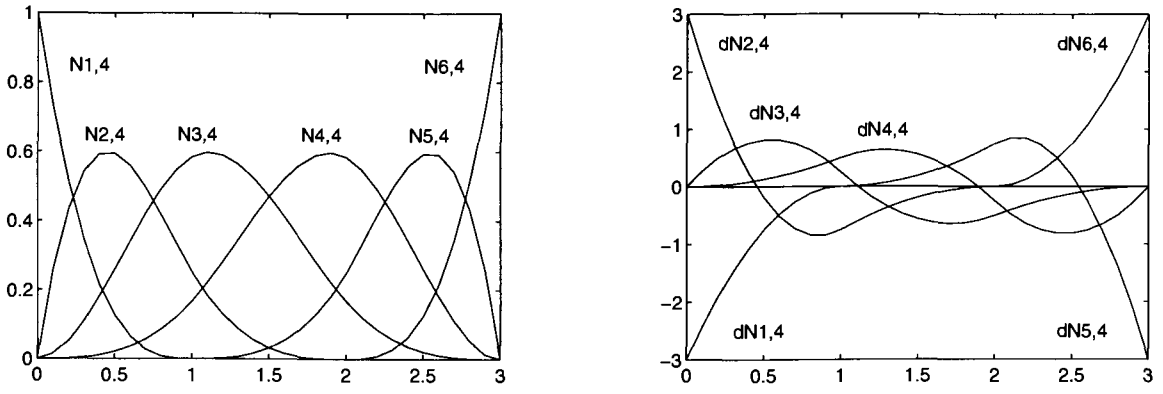

Fig. 51. Basis functions and 1st dervatives for a 4th order B-spline with uniform knot spacing

A.1.3 Properties of B-Spline Basis Functions

The following are some properties of the normalized B-spline basis functions:

- Positivity:

$$N_{i,k}(x) \geq 0 \qquad \text{for all} x \tag{71}$$

- Sum:

$$\sum_{i=1}^{n+1} N_{i,k}(x) = 1 \tag{72}$$

- Derivative of a B-spline basis function:

$$N'_{i,k}(x) = \frac{N_{i,k-1}(x) + (x-\lambda_i)N'_{i,k-1}(x)}{\lambda_{i+k-1}-\lambda_i} - \frac{(\lambda_{i+k}-x)N'_{i+1,k-1}(x) - N_{i+1,k-1}(x)}{\lambda_{i+k}-\lambda_{i+1}} \tag{73}$$

- 2nd derivative of a B-spline basis function:

$$N''_{i,k}(x) = \frac{2N'_{i,k-1}(x) + (x-\lambda_i)N''_{i,k-1}(x)}{\lambda_{i+k-1}-\lambda_i} - \frac{(\lambda_{i+k}-x)N''_{i+1,k-1}(x) - 2N'_{i+1,k-1}(x)}{\lambda_{i+k}-\lambda_{i+1}} \tag{74}$$

The convention 0/0 = 0 is adopted for the above equations. It is never the case that the numerator is nonzero when the denominator is zero.

A.2 Bivariate B-splines

Consider a tensor product spline of order k in the x direction and of order l in the y direction. There are $k+n+1$ knot values specified in the x direction $\lambda_0, \ldots, \lambda_{k+n}$, and $l+m+1$ knot values are specified in the y direction $\mu_0, \ldots, \mu_{l+m}$. The B-spline coefficients which define the control points are $c_{i,j}$. The basis functions are N and M in x and y respectively.

$$S(x, y) = \sum_{i=1}^{n+1} \sum_{j=1}^{m+1} c_{i,j} N_{i,k}(x) M_{j,l}(y) = z \tag{75}$$

The pth partial derivative in x and qth partial derivative in y is:

$$\frac{\partial^{p+q}}{\partial x^p \partial y^q} S(x, y) = \sum_{i=1}^{n+1} \sum_{j=1}^{m+1} c_{i,j} N_{i,k}^{(p)}(x) M_{j,l}^{(q)}(y) \tag{76}$$

Appendix B - Equations for Paraboloid

The paraboloid was formed by rotating the curve $z = -Cx^2$ about the z-axis.

The map for the paraboloid with parameter C is chosen to be:

$$f(u, v) = \begin{bmatrix} u \\ v \\ -C\left(u^2 + v^2\right) \end{bmatrix} \qquad \{ (u, v) \mid (-2 < u < 2, -2 < v < 2) \} \tag{77}$$

The Gauss map for the above surface map is unknown and will be calculated as the cross product of $x(u, v)$ and $y(u, v)$. As mentioned earlier, the Gauss map $g(f(u, v))$, maps the point on the surface defined by $f(u, v)$ to the surface normal at that point.

The partial derivatives of $f(u, v)$ and their magnitudes are:

$$\begin{aligned} f_u(u, v) &= (1, 0, -2Cu) & f_v(u, v) &= (0, 1, -2Cv) \\ \left\| f_u(u, v) \right\| &= \sqrt{1 + (-2Cu)^2} & \left\| f_v(u, v) \right\| &= \sqrt{1 + (-2Cv)^2} \end{aligned} \tag{78}$$

Solving the above equations for the coordinate axes at the point of contact for the paraboloid results in the following equations:

$$x(u, v) = \begin{bmatrix} \dfrac{1}{\sqrt{1 + (-2Cu)^2}} \\ 0 \\ \dfrac{-2Cu}{\sqrt{1 + (-2Cu)^2}} \end{bmatrix} \qquad y(u, v) = \begin{bmatrix} 0 \\ \dfrac{1}{\sqrt{1 + (-2Cv)^2}} \\ \dfrac{-2Cv}{\sqrt{1 + (-2Cv)^2}} \end{bmatrix} \tag{79}$$

$$z(u,v) = x(u,v) \times y(u,v) = \begin{bmatrix} \left(\frac{2Cu}{\sqrt{1+(-2Cu)^2}} \cdot \frac{1}{\sqrt{1+(-2Cv)^2}}\right) \\ \left(\frac{-1}{\sqrt{1+(-2Cu)^2}} \cdot \frac{-2Cv}{\sqrt{1+(-2Cv)^2}}\right) \\ \left(\frac{1}{\sqrt{1+(-2Cu)^2}} \cdot \frac{1}{\sqrt{1+(-2Cv)^2}}\right) \end{bmatrix} \tag{80}$$

The metric for the surface is used to measure the changes in the position on the surface for a differential change in the parameters u and v. The metric for the paraboloid is:

$$M_2 = \begin{bmatrix} \sqrt{1+(-2Cu)^2} & 0 \\ 0 & \sqrt{1+(-2Cv)^2} \end{bmatrix} \tag{81}$$

The curvature form (K_2) for the paraboloid is calculated as before. The intermediate calculations are shown below:

$$\frac{z_u(u,v)}{\|f_u(u,v)\|} = \frac{1}{\left(1+(-2Cu)^2\right)^2\sqrt{1+(-2Cv)^2}} \begin{bmatrix} 2C \\ -8C^3uv \\ -4C^2u \end{bmatrix} \tag{82}$$

$$\frac{z_v(u,v)}{\|f_v(u,v)\|} = \frac{1}{\sqrt{1+(-2Cu)^2}\left(1+(-2Cv)^2\right)^2} \begin{bmatrix} -8C^3uv \\ 2C \\ -4C^2v \end{bmatrix} \tag{83}$$

The curvature form of the paraboloid is:

$$K_2 = \begin{bmatrix} \frac{2C}{\left(1+(-2Cu)^2\right)^{\frac{3}{2}}\sqrt{1+(-2Cv)^2}} & 0 \\ 0 & \frac{2C}{\sqrt{1+(-2Cu)^2}\left(1+(-2Cv)^2\right)^{\frac{3}{2}}} \end{bmatrix} \tag{84}$$

The quantities required in the calculation of the torsion form are:

$$x_u(u,v) = \begin{bmatrix} \left(\dfrac{-4C^2u}{\left(1+(-2Cu)^2\right)^{\frac{3}{2}}}\right) \\ 0 \\ \left(\dfrac{2C}{\sqrt{1+(-2Cu)^2}} + \dfrac{8C^3u^2}{\left(1+(-2Cu)^2\right)^{\frac{3}{2}}}\right) \end{bmatrix} \qquad x_v(u,v) = \begin{bmatrix} 0 \\ 0 \\ 0 \end{bmatrix} \tag{85}$$

$$\frac{x_u(u,v)}{\|f_u(u,v)\|} = \begin{bmatrix} \dfrac{-4C^2u}{\left(1+(-2Cu)^2\right)^2} \\ 0 \\ \dfrac{-2C}{\left(1+(-2Cu)^2\right)^2} \end{bmatrix} \tag{86}$$

The torsion form of the for the paraboloid is:

$$T = \left[\frac{4C^2v}{\left(1+(-2Cu)^2\right)^2\sqrt{1+(-2Cv)^2}}, \quad 0\right] \tag{87}$$

Bibliography

[1] P. K. Allen and P. Michelman, "Acquisition and Interpretation of 3-D Sensor Data from Touch", IEEE T. on Robotics & Automation, Vol. 6, No. 4, pp. 397-404, 1987

[2] P. K. Allen, "Object Recognition Using Active Tactile Sensing", Advanced Tactile Sensing for Robotics, Howard R. Nicholls, World Scientific, 1992

[3] Assurance Technologies, Inc., "Installation and Operations Manual for F/T", PN 9610-05-1001-01, Appendix A

[4] R. C. Beach, "An Introduction to the Curves and Surfaces of Computer Aided Design", Van Nostrand Reinhold, New York, 1991

[5] F. P. Beer and E. R. Johnston, Jr., "Vector Mechanics for Engineers: Statics and Dynamics", McGraw-Hill, Inc., Montreal, 1984

[6] P. J. Besl, "Surfaces in Range Image Understanding", Springer-Verlag, New York, 1988

[7] B. Bhanu and Chih-Cheng Ho, "CAD-Based 3D Object Representation for Robot Vision", IEEE ICRA, pp. 19-35, August 1987

[8] C. de Boor, "A Practical Guide to Splines", Springer-Verlag, New York, 1978

[9] C. Cai and B. Roth, "On the planar motion of rigid bodies with point contact", Mechanism and Machine Theory, 21(6):453-466, 1986

[10] M. Charlebois, K. Gupta, and S. Payandeh, "Curvature Based Shape Description Using Tactile Sensing", IEEE ICRA, Vol X, pp. 3502-3507, 1996

[11] S. J. Dickinson, A. P. Pentland, and A. Rosenfeld, "A Representation for Qualitative 3-D Object Recognition and Viewer-Centered Models.", Science of Vision, K.N Leibovic, Springer Verlag, pp. 398-421, 1990

[12] P. Dierckx, "Curve and Surface Fitting with Splines", Clarendon Press, New York, 1993

[13] J. C. Dill, "An application of Color Graphics to the Display of Surface Curvature", Computer Graphics, Vol. 15, No. 3, August 1981

[14] G. Elber and E. Cohen, "Second-Order Surface Analysis Using Hybrid Symbolic and Numeric Operators", ACM Transactions on Graphics, Vol. 12, No. 2, pp. 160-178, April 1993

[15] R. S. Fearing, "Tactile Sensing for Shape Interpretation", Dexterous Robot Hands, S. T. Venkataraman and T. Iberall, Springer-Verlag, 1990

[16] R. Fearing and T. Binford, "Using a Cylindrical tactile sensor for determining curvature", IEEE Trans. on Robotic and Automation, 7(6):806-817, 1991

[17] J. Foley, A. van Dam, S. Feiner, J. Hughes, " Computer Graphics Principles and Practice. Second Edition", Addison-Wesley, 1990.

[18] S. I. Grossman, "Calculus Fourth Edition", Harcourt Brace Jovanovich, 1988

[19] H. Hemami, J. Bay, and R. E. Goddard, "A Conceptual Framework for Tactually Guided Exploration and Shape Perception", IEEE Transactions on Biomed. Eng., Vol. 35, No. 2, p. 99-109, Feb 1988

[20] R. Joshi and A. C. Sanderson. "Shape Matching from Grasp Using a Minimal Representation Size Criterion", IEEE ICRA, Vol. 1, pp. 442-449, 1993

[21] J. J. Koenderink, "Solid Shape", The MIT Press, Cambridge, M.A., 1990

[22] S. J. Lederman, R. L. Klatzky and D. T. Pawluk, "Lessons From the Study of Biological Touch for Robotic Haptic Sensing", Advanced Tactile Sensing for Robotics, H. R. Nicholls, World Scientific, 1992

[23] D. Montana, "The Kinematics of Contact and Grasp", The Int'l J. of Robotics Research, Vol. 7, No. 3, p. 17-31, June 1988

[24] K. Roberts, "Robot Active Touch Exploration: Constraints and Strategies," IEEE ICRA, Vol. 2, p. 980-5, 1990

[25] D.F. Rogers and J. A. Adams, "Mathematical Elements for Computer Graphics", McGraw-Hill, New York, 1990

[26] S. S. Sinha and P. J. Besl, "Principal Patches a Viewpoint Invariant Surface Description", IEEE ICRA, Vol. 1, pp. 226-231, 1990

[27] M. Spong and M. Vidyasagar, "Robot Dynamics and Control", Wiley, 1989

[28] E. Trucco and Robert B. Fisher, "Experiments in Curvature-Based Segmentation of Range Data", IEEE PAMI, Vol. 17, No. 2, p. 177-182, Feb 1995

[29] T. Tsujimura and T. Yabuta, "Object Detection by Tactile Sensing Method Employing Force/Torque Information", IEEE Transactions on Robotics and Automation, Vol. 5, No. 4, August 1989

[30] N. Yokoya and M. D. Levine, "Range Image Segmentation Based on Differential Geometry: A Hybrid Approach", IEEE Transactions on PAMI, Vol. 11, No. 6, pp. 643-649, June 1989